Extreme Low-Level Updrafts and Wind Speeds Measured by Dropsondes in Tropical Cyclones

DANIEL P. STERN AND GEORGE H. BRYAN

National Center for Atmospheric Research,[a] Boulder, Colorado

SIM D. ABERSON

NOAA/AOML/Hurricane Research Division, Miami, Florida

(Manuscript received 10 September 2015, in final form 22 March 2016)

ABSTRACT

Previous studies have found surprisingly strong vertical motions in low levels of some tropical cyclones. In this study, all available dropsondes (~12 000) within tropical cyclones during 1997–2013 are examined, in order to create a dataset of the most extreme updrafts (≥10 m s^{-1}; 169 sondes) and wind speeds (≥90 m s^{-1}; 64 sondes). It is shown that extreme low-level (0–3 km) updrafts are ubiquitous within intense (category 4 and 5) tropical cyclones, and that few such updrafts have been observed within weaker storms. These extreme updrafts, which are almost exclusively found within the eyewall just inward of the radius of maximum winds, sometimes occur in close association with extreme horizontal wind speeds. Consistent with previous studies, it is suggested that both the extremes in vertical velocity and wind speed are associated with small-scale (~1 km) vortices that exist along the eye–eyewall interface. As a substantial number of updrafts are found within a kilometer of the surface, it can be shown that it is implausible for buoyancy to be the primary mechanism for vertical acceleration. Additionally, the azimuthal distribution of both the extreme updrafts and wind speeds is strongly associated with the orientation of the environmental vertical wind shear.

1. Introduction

Since the introduction of the GPS dropwindsonde (hereafter "dropsonde" or "sonde") in 1997 (Hock and Franklin 1999), roughly 12 000 dropsondes have been released into tropical cyclones (TCs) (Wang et al. 2015), by both research (NOAA P3) and operational [U.S. Air Force (USAF) C130] aircraft. Although it has not been widely utilized for this purpose, dropsondes are capable of retrieving vertical (in addition to horizontal) wind speeds (e.g., Wang et al. 2009). The vast majority of dropsondes sample relatively weak vertical motions, and even sondes released within the eyewall of tropical cyclones rarely sample updrafts stronger than 5 m s^{-1}. This is consistent with the fact that deep convection within tropical cyclones (and tropical oceanic convection in general) is typically much weaker than within mid-latitude continental thunderstorms (LeMone and Zipser 1980; Zipser and LeMone 1980; Jorgensen et al. 1985; Jorgensen and LeMone 1989; Black et al. 1996; Zipser et al. 2006). Nevertheless, relatively strong vertical motions have been found to occur within some tropical cyclones (Black et al. 1994, 1996; Marks et al. 2008; Guimond et al. 2010; Heymsfield et al. 2010). These observational studies of vertical motion in tropical cyclones have found that updrafts of 10–30 m s^{-1} can occur. Such studies were based on either flight-level data or Doppler radar, and primarily focused on updrafts in mid- and upper levels. Dropsondes, however, are a crucial tool for understanding what is occurring at low levels, and in particular, within the boundary layer.

Stern and Aberson (2006) presented a preliminary analysis of a dataset containing all dropsondes from 1997 to 2005 that experienced updrafts strong enough such that the sonde began to rise. This situation occurs when the upward speed of the air exceeds the terminal fall

[a] The National Center for Atmospheric Research is sponsored by the National Science Foundation.

Corresponding author address: Daniel P. Stern, University Corporation for Atmospheric Research, 7 Grace Hopper Ave., Monterey, CA 93943.
E-mail: dstern@ucar.edu

DOI: 10.1175/MWR-D-15-0313.1

speed of the sonde, which is 10–13 m s^{-1} at the altitudes sampled (generally below 2–3-km height, the most typical flight levels). Stern and Aberson (2006) termed these "upsondes," and they identified 77 such dropsondes, in 19 different tropical cyclones. They found that upsondes were almost exclusively a phenomenon of the eyewall of the strongest hurricanes, with 90% of the dataset coming from category 4 or 5 hurricanes. Additionally, they showed that the vertical shear of the environmental horizontal winds had a very strong relationship with the location of the updrafts, with 90% of the upsondes occurring in the left-of-shear semicircle. The extreme updrafts were found both above and within the boundary layer, and sometimes only 100 m above the surface.

Stern and Aberson (2006) noted that a substantial number of sondes that sampled extreme updrafts also sampled extreme horizontal wind speeds, which were defined by Aberson and Stern (2006) as values $\geq$90 m s^{-1}. Here, we extend the preliminary datasets of Stern and Aberson (2006) and Aberson and Stern (2006) through 2013, and provide a more comprehensive analysis. For reasons described below, we consider all dropsondes that sampled updrafts exceeding 10 m s^{-1}, instead of the original upsonde criterion of Stern and Aberson (2006). Stern and Aberson (2006) speculated that these extreme updrafts may result from thermal buoyancy associated with enhanced convective available potential energy (CAPE), supporting the hypothesis of Aberson et al. (2006). Upon further consideration, and based on this more comprehensive observational analysis, we no longer believe that these extreme low-level (below 1–2 km) updrafts are substantially driven by buoyancy, and here we will advance the argument that the extreme vertical accelerations needed to produce these updrafts so close to the surface (within the lowest 1–2 km) can only be due to dynamical nonhydrostatic pressure gradients.

Understanding the frequency, structure, and dynamics of these extreme low-level updrafts is important, for several reasons. 1) We suspect that such updrafts are associated with the existence of localized extreme near-surface winds, and that both the updrafts and extreme wind speeds may be associated with kilometer-scale vortices that exist along the eye–eyewall interface. Aberson et al. (2006) and Marks et al. (2008) presented strong evidence for the existence of such vortices; our results here support these prior studies, and we will show that extreme low-level updrafts are common in intense hurricanes. 2) To the extent that the updrafts are associated with coherent vortices, these features may represent a mechanism by which localized extreme damage is produced in landfalling TCs (Wakimoto and Black 1994; Powell and Houston 1996). 3) Intense TCs also pose a substantial risk to offshore wind turbines (Rose et al. 2012), and it is important to be able to better quantify the risk of turbines encountering such extreme local wind maxima. 4) In addition to this broader societal relevance, from the perspective of aircraft safety, it is important to better understand the frequency, magnitude, and spatial distribution of extreme low-level updrafts. As discussed in Marks et al. (2008), a NOAA P3 aircraft encountered severe turbulence in association with extreme updrafts in the eyewall of Hurricane Hugo (1989), resulting in engine failure and a near catastrophe. As a result of this flight, aircraft are no longer allowed to penetrate the eyewall at such low altitudes (500 m) in intense TCs. We now know (e.g., Lorsolo et al. 2010; Zhang et al. 2011) that the boundary layer within the eyewall of intense TCs is typically quite turbulent. However, it remains unknown how frequently an aircraft might be expected to encounter a feature similar to that observed in Hugo, and how these features vary as a function of height and TC intensity. 5) Finally, it has been suggested that the features that we observe here may affect the overall (e.g., 1-min average) TC intensity, although there remains disagreement as to whether the effect is positive (Persing et al. 2013) or negative (Rotunno et al. 2009). While we are unable to fully address the above questions from the observations alone, this study provides a first step toward understanding the frequency, structure, and dynamics of extreme updrafts and wind speeds in tropical cyclones.

2. Data and methodology

NOAA's Hurricane Research Division (HRD) maintains an online archive of all NOAA and USAF dropsondes released within Atlantic and east Pacific tropical cyclones, as well as some west Pacific TCs (from special field programs). For each dropsonde, an Airborne Vertical Atmospheric Profiling System (AVAPS) file is produced (in real time on the aircraft), which contains the raw wind and thermodynamic data. We acquired all available AVAPS files for sondes that were dropped within tropical cyclones. Note that we only considered sondes dropped during NOAA P3 and USAF C130 flights; NOAA GIV flights generally are restricted to the environment of TCs (often at least several hundred kilometers from the storm center), and sondes that were dropped within some TCs by NASA aircraft are not present in the HRD archive. After acquiring the AVAPS files, we then used NCAR's Atmospheric Sounding Processing Environment (ASPEN) software[1] to postprocess and quality control the data. ASPEN has

[1] Additional information on ASPEN can be found online at https://www.eol.ucar.edu/content/aspen.

the capability of sequentially and automatically processing numerous sondes and, as a "screening step," we first processed all available AVAPS files (from 1997 to 2013) from P3 and C130 flights using this "batch mode," and searched for the maximum updraft and horizontal wind speed for each sonde, making note of all sondes that appeared to sample updrafts exceeding $10\,\mathrm{m\,s^{-1}}$ and/or horizontal wind speeds exceeding $90\,\mathrm{m\,s^{-1}}$.

While ASPEN applies a number of quality-control algorithms to automatically find and remove erroneous or suspicious data points, it is still quite common for a sonde to require manual quality control as well. This manual intervention can involve (among other things): removing bad data points, removing bad flight-level data, or determining that the sonde failed prior to reaching the surface. This latter occurrence is particularly important, as the height data in ASPEN are determined not by the GPS-measured height, but by upward integration of the hydrostatic equation, with the assumption that the final (in time) data point corresponds to the surface. If the final data point is actually from some height substantially above the surface, then the computed heights from upward integration will be erroneous. If it is clear that the sonde failed prior to reaching the surface, then the flight-level data can be used for a downward integration of the hydrostatic equation, assuming that the flight-level data are available and reliable.

After identifying candidate sondes for our dataset, we then individually reprocessed and carefully examined each such sonde, making corrections to the automatic ASPEN quality control as necessary, and discarding sondes whose apparent extreme updrafts/wind speeds were spurious. One rather common cause of spurious updrafts are sondes whose release time is misidentified (either in the raw data or by ASPEN) as occurring prior to the exit of the sonde from the aircraft. This leads to apparent horizontal wind speeds equal to the speed of the plane and vertical velocity equal in magnitude to the terminal fall speed of the sonde.

The preliminary datasets of Stern and Aberson (2006) and Aberson and Stern (2006) were quality controlled using HRD's Editsonde software. ASPEN is based in part on Editsonde, and so their quality-control algorithms are generally similar, though not identical. As Editsonde was developed on a specific (and deprecated) computer architecture, it can no longer be run. Therefore, in order to create a homogeneous dataset that extended through the end of 2013, we decided to use ASPEN to reprocess all of the sondes in the preliminary dataset. This led to some minor differences in the profiles of the original upsondes, in particular for vertical velocity. This is because the calculated vertical velocity of the air, w_{air}, is a function of the theoretical terminal fall speed of the sonde, w_{fall}, which depends on the mass of the sonde, m_s, through the following formula:

$$w_{\mathrm{fall}} = [2m_s g/(C_{\mathrm{ds}} A_s \rho)]^{1/2}, \tag{1}$$

where g is the gravitational acceleration, C_{ds} is the drag coefficient of the sonde [determined from wind tunnel measurements (Wang et al. 2009)], A_s is the area of the parachute, and ρ is the density of the air. Here we use $C_{\mathrm{ds}} = 0.61$, $A_s = 0.09\,\mathrm{m^2}$, $g = 9.81\,\mathrm{m\,s^{-2}}$, and ρ is calculated from the temperature T and pressure p measured by the sonde (the effect of moisture is neglected). Note that Wang et al. (2009) give a value of $0.0676\,\mathrm{m^2}$ for A_s. It is unclear whether they were using sondes with smaller parachutes or if the cited value is incorrect. We also note that C_{ds} was determined for a specific model of the Vaisala GPS dropsonde (RD93). The current model (RD94) likely has a slightly different C_{ds}, although the value is unknown (K. Young 2013, personal communication). Finally, Editsonde uses a value of $C_{\mathrm{ds}} = 0.63$, and this has a slight (a few percent) effect on derived vertical velocities.

In 2010, a redesigned dropsonde (RD94) was introduced, replacing the original model (RD93) that was described in Hock and Franklin (1999). RD94 is lighter (322 g) than RD93 (389 g), and so its terminal fall speed is slower, by about $1\,\mathrm{m\,s^{-1}}$ for near-surface air densities. As a result, the threshold updraft at which a sonde begins to rise instead of fall varies within our dataset. Although this difference is small relative to the updraft magnitudes we are considering, we decided that it would be best to no longer use the upsonde criterion of Stern and Aberson (2006) to define our dataset of extreme updrafts. Instead, we use a fixed threshold vertical velocity (of the air) of $10\,\mathrm{m\,s^{-1}}$. In general, this slightly relaxes the criterion of Stern and Aberson (2006). Counteracting this effect is the fact that a mass of 420 g was assumed for the upsonde dataset processed with Editsonde, and this resulted in a derived updraft velocity that is slightly greater than what we now believe to be correct. Ultimately, w_{fall} is somewhat uncertain, as (1) is semiempirical; in addition, there may have been variations in sonde mass and parachute size among different versions of the dropsonde, and these are poorly documented or unknown (M. Black 2013, personal communication). An additional uncertainty is introduced by the use of pressure changes to determine vertical velocity through the hydrostatic equation, as extreme updrafts are almost certainly nonhydrostatic. Using ASPEN, we compared the GPS-derived to the pressure-derived vertical velocity, and ensured that no cases exhibited large discrepancies between the two measurements. As

TABLE 1. List of TCs in the w10 dataset. TCs in the east and west Pacific are denoted parenthetically by EP and WP, respectively. "No. of total sondes" refers to the number of sondes from all flights for a given storm that contributed at least one w10 sonde.

Year	Storm name	No. of w10 sondes	No. of total sondes	Fraction of w10 sondes
1997	Guillermo (EP)	1	9	0.11
1998	Georges	4	57	0.07
1998	Mitch	3	51	0.06
1999	Bret	2	22	0.09
1999	Floyd	6	65	0.09
1999	Lenny	1	16	0.06
2000	Keith	1	8	0.13
2001	Juliette (EP)	1	11	0.09
2001	Iris	5	24	0.21
2001	Michelle	3	29	0.10
2002	Kenna (EP)	2	24	0.08
2002	Lili	9	90	0.10
2003	Claudette	1	7	0.14
2003	Fabian	2	42	0.05
2003	Isabel	13	167	0.08
2004	Bonnie	1	8	0.13
2004	Charley	5	36	0.14
2004	Frances	6	97	0.06
2004	Ivan	40	344	0.12
2005	Dennis	12	83	0.14
2005	Emily	15	81	0.19
2005	Katrina	6	61	0.10
2005	Rita	7	114	0.06
2005	Wilma	4	70	0.06
2006	Ernesto	1	12	0.08
2006	Florence	1	7	0.14
2007	Dean	5	33	0.15
2007	Felix	2	9	0.22
2008	Ike	1	7	0.14
2008	Jangmi (WP)	1	39	0.03
2008	Paloma	1	28	0.04
2009	Bill	1	20	0.05
2010	Earl	2	34	0.06
2010	Paula	2	8	0.25
2010	Megi (WP)	2	53	0.04

pressure is more accurate than GPS height, only the pressure-derived vertical velocities are output by ASPEN in the quality-controlled soundings. We estimate that the uncertainty in vertical velocity is on the order of $1\,m\,s^{-1}$ (see the appendix), and so while dropsondes cannot reliably be used to assess weak vertical velocities (i.e., in the periphery of the storm or in the eye), the extreme updrafts that we examine here are likely robust.

Our dataset of $\geq 10\,m\,s^{-1}$ updrafts (hereafter "w10") consists of 169 dropsondes within 35 tropical cyclones. The dataset of $\geq 90\,m\,s^{-1}$ wind speeds (hereafter "ws90") consists of 64 sondes within 12 tropical cyclones. The w10 and ws90 datasets represent approximately 1.5% and 0.5% of all TC dropsondes, respectively. A list of the storms represented in each dataset is given in Tables 1 and 2 respectively. Note that 56 (88%) of the ws90 sondes are from just 4 years (2003, 2004, 2005, and 2010), and that 8 of the 17 years are not represented in the dataset. While the w10 dataset is somewhat more evenly distributed, 96 (57%) of the sondes are from 2004 and 2005, and there are no such sondes from 2011 to 2013. There are several reasons for this characteristic of the distribution, but the most important is that extreme updrafts and (in particular) extreme wind speeds are much more common in very strong TCs, and some years have few or no such storms in the Atlantic basin. As we will later discuss, nearly all well-observed category 4 and 5 hurricanes contain at least one sonde that sampled an updraft in excess of $10\,m\,s^{-1}$.

Note that the plotted data for the following figures in this study are generally not homogeneous (i.e., the number of valid data points varies among data sources and variables). For example, height data are missing for at least a portion of many sonde profiles, and some sondes were dropped at a time for which there is no accurate flight-level data. The number of data points for each plotted variable is given in the figure captions.

TABLE 2. List of TCs in the ws90 dataset. TCs in the east and west Pacific are denoted parenthetically by EP and WP, respectively. "No. of total sondes" refers to the number of sondes from all flights for a given storm that contributed at least one ws90 sonde.

Year	Storm name	No. of ws90 sondes	No. of total sondes	Fraction of ws90 sondes
1998	Mitch	4	40	0.10
1999	Lenny	1	7	0.14
2002	Kenna (EP)	1	13	0.18
2003	Isabel	17	124	0.14
2004	Ivan	12	83	0.14
2005	Emily	1	13	0.08
2005	Katrina	6	47	0.13
2005	Rita	6	44	0.14
2007	Dean	1	13	0.08
2007	Felix	1	5	0.20
2008	Jangmi (WP)	2	39	0.05
2010	Megi (WP)	12	78	0.15

3. Relationship of extreme updrafts and wind speeds with TC intensity and intensity change

Extreme low-level updrafts are found almost exclusively in major hurricanes (categories 3, 4, and 5; maximum 1-min winds at 10-m height $\geq$ 96 kt, 1 kt = 0.5144 m s^{-1}), as shown in Fig. 1a. Specifically, 92% (155/169) of sondes that sampled extreme updrafts are found in major hurricanes, and 79% (134/169) are from category 4 and 5 storms. Here, we interpolate the best track (Landsea and Franklin 2013) intensity to the time each sonde was dropped. There are a few extreme updrafts found at much weaker intensities. Nevertheless, it is clear that the frequency of extreme low-level updrafts in tropical cyclones increases markedly with increasing intensity. Figure 1b shows the frequency of extreme horizontal wind speeds as a function of best track intensity. All such sondes are from storms with intensity in excess of 130 kt. This is not surprising, as the mean storm intensity must already be very strong in order to produce local winds in excess of 90 m s^{-1}.

Figures 1c and 1d show scatterplots of the maximum vertical velocity and the maximum horizontal wind speed versus the best track intensity for the w10 and ws90 sondes, respectively. There does not appear to be a systematic relationship between the value of either maximum and the storm intensity. Perhaps this lack of relationship indicates that there is some threshold of intensity beyond which extreme updrafts and wind speeds become much more likely, but that once this threshold is exceeded, there is little dependence of the strength of the updraft and wind speed perturbations on the mean wind speed. On the other hand, it is very possible that the lack of relationship is a consequence of limited sampling (Jorgensen et al. 1985; Uhlhorn and Nolan 2012). In particular, we expect there to be a relationship between the maximum observed wind gust and the best track intensity, and the fact that we do not clearly see such a relationship in Fig. 1d suggests that limited sampling is likely the primary reason. It is possible that errors in determining the best track intensity also contribute to the lack of relationship between intensity and the magnitude of the extremes. Note that the dropsonde maximum wind speed is representative of a gust on the scale of a few seconds, whereas the best track intensity is intended to be representative of the maximum 1-min average wind speed. Further, the dropsonde maximum occurs above the surface, whereas the best track intensity is defined to be valid at the surface (10 m). For these reasons, the peak dropsonde wind speed is not directly comparable to the best track intensity. Nevertheless, it is expected that there should be some relationship between the two. We plan to use high-resolution model simulations to examine this issue in a future study.

Some studies have suggested that the strongest updrafts tend be found in rapidly intensifying storms (Jorgensen et al. 1985; Black et al. 1994). Figure 2a shows a histogram of the 6-h best track intensity change (calculated from the two analysis times that bound the drop time of each sonde) for the w10 sondes. Aside from a few storms that were rapidly weakening due to landfall within a few hours of sampling (Kenna, Charley, Dennis, and Dean) and a small number of cases with quite large 6-h intensity increases, most of the extreme updrafts are found at times that storms are undergoing relatively small intensity change. The distribution is biased slightly toward intensification, but so is the distribution of intensity change for all storms (Kaplan and DeMaria 2003). We also looked at the intensity change in the 12- and 24-h periods subsequent to the drop time (not shown), and in these analyses, the distribution is actually biased toward weakening, perhaps because many of these storms are near to their maximum

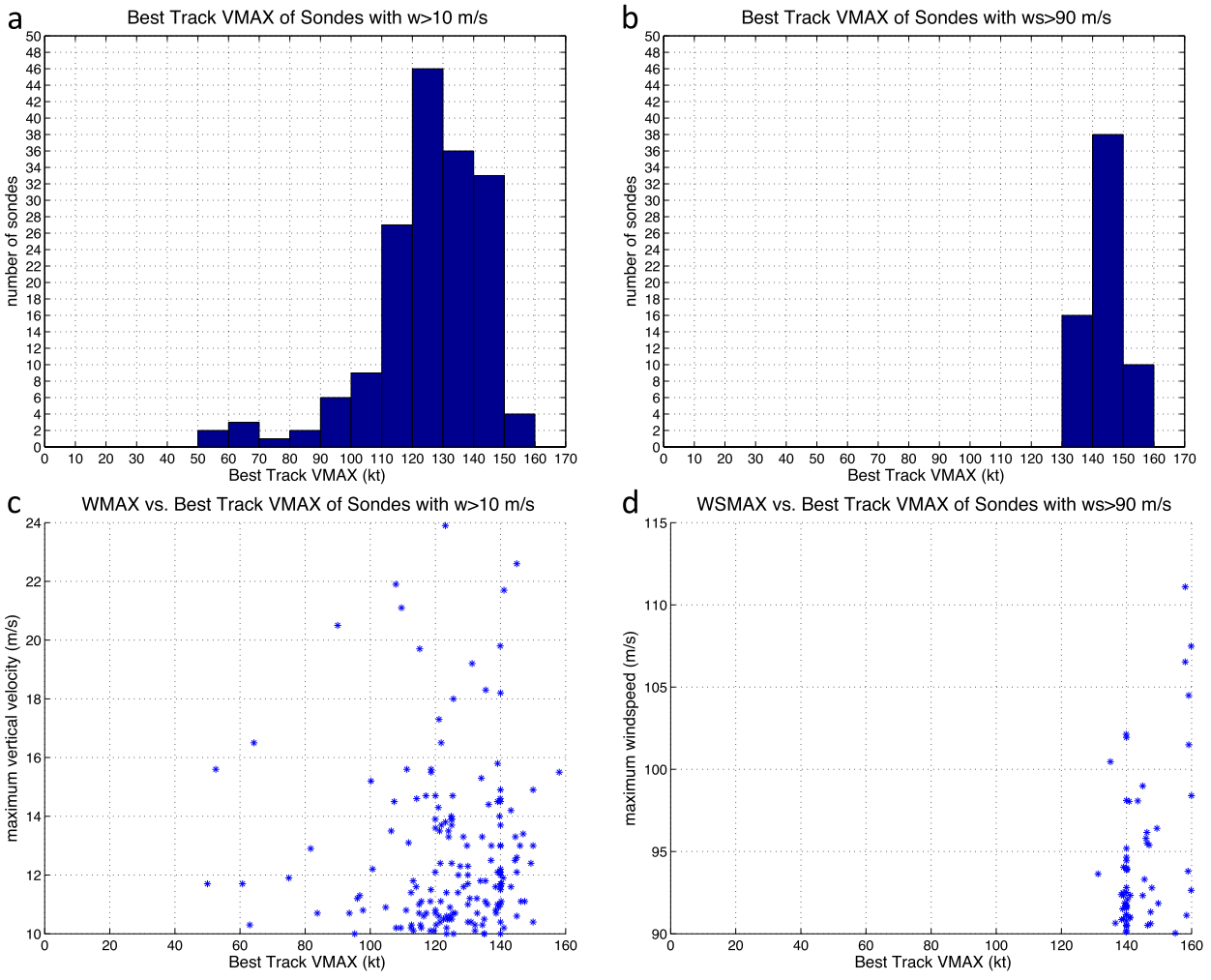

FIG. 1. Histograms of the number of sondes in the (a) w10 and (b) ws90 datasets vs best track Vmax (kt). Scatterplots of the (c) maximum vertical velocity ($m\,s^{-1}$) and (d) maximum wind speed ($m\,s^{-1}$) vs best track Vmax (kt) for the sondes in the w10 and ws90 datasets, respectively. For (a),(b), and (d), all sondes are shown. For (c), one sonde whose measured wmax is less than $10\,m\,s^{-1}$ is not plotted (due to missing data; it can be inferred that wmax exceeds $10\,m\,s^{-1}$, as the sonde rises).

potential intensity. While the existence of several very rapidly intensifying storms in the 6-h period encompassing the drops implies that there may be some relationship between intensity change and extreme updrafts, a comparison of Figs. 2a and 1a suggests that extreme low-level updrafts are much more related to intensity itself, rather than intensity change. Indeed, all of the storms (in this dataset) with 6-h intensity change of 15 kt or greater had best track intensities exceeding 90 kt (not shown). If intensity change were very important, we might expect to see more sondes from weaker but rapidly intensifying storms, or fewer sondes from weakening or steady-state storms. The fact that we do not see these latter scenarios is evidence that peak low-level updraft strength in tropical cyclones is most related to storm intensity itself.

Figure 2b is similar to Fig. 2a, but for the ws90 sondes. As with the w10 sondes, most ws90 sondes are found at times of small intensity change, and the distribution is slightly biased toward intensifying storms. Despite the already strong intensity of the storms in the ws90 dataset, a few sondes are found at times where storm intensity increases by greater than 15 kt in 6 h.

4. Spatial distribution of extreme updrafts and wind speeds

a. Heights of the maximum updraft and horizontal wind speed

Figure 3a shows a histogram of the heights where the maximum updrafts occur for the w10 sondes. The height

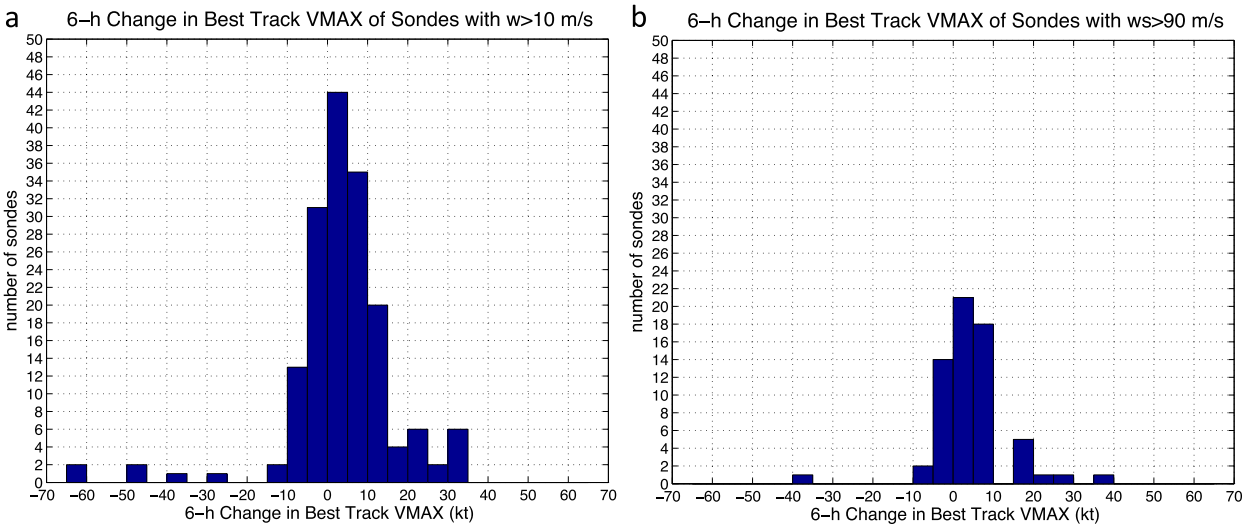

FIG. 2. Histograms of the number of sondes in the (a) w10 and (b) ws90 datasets vs the 6-h change in best track Vmax (kt). The 6-h change is given by the difference between Vmax at the two best track times that bound the time each sonde was dropped. For both (a) and (b), all sondes are shown.

of maximum updraft is quite variable, with a number of sondes possessing a maximum just below flight level (flight level varies from 1.5 to 4.5 km, but for most cases is between 2 and 3 km), while some other sondes sample extreme updrafts in the lowest few hundred meters above the surface. Note that the sharp drop-off in sondes above 3 km is due to a lack of flights above this height, and so we cannot determine with this dataset how the frequency of extreme updrafts truly varies with height in this region. Below 3 km, some of the variability may be a function of the radial location of the drop relative to the radius of maximum wind (RMW) and of the degree to which the RMW slopes outward with height. For example, if a sonde is dropped at, or immediately inward of, the flight-level RMW, the sonde may sample the strongest updraft at or just below flight level, whereas if the sonde is dropped just a few kilometers farther inward (10–20 s of flight time), the strongest updraft may be sampled much closer to the surface. In addition, there is likely substantial small-scale spatial variability of the vertical velocity. Unfortunately, without knowledge of the three-dimensional wind field, it is very difficult to determine which of these factors is more important. Therefore, we are unable to determine whether the apparent maximum between 500- and 1000-m height reflects the true height of peak frequency of extreme low-level updrafts, or instead these sampling artifacts. In any case, it is clear that extreme updrafts are found over a broad range of heights, including very close to the surface. Note that here (and elsewhere), we are specifically examining the location of the *maximum*; updrafts can still exceed 10 m s^{-1} at heights substantially below that of the peak, and in many cases, there exist multiple distinct local maxima (not shown).

The heights where extreme horizontal wind speeds are found (Fig. 3b) is more restricted than that of the extreme updrafts. The heights of the maximum wind speed for the ws90 sondes are all below 1500 m, and 36% (20/56) are found between 400- and 600-m height. This is broadly consistent with previous studies that indicate that the maximum winds in tropical cyclones are, on average, found at about 500 m (Franklin et al. 2003). Nevertheless, there are a number of ws90 sondes in which maximum winds are found much closer to the surface, including seven sondes with maxima below 200-m height.

Figure 3c shows the histogram of the maximum vertical velocity for the w10 sondes. Slightly greater than half of the dataset is composed of sondes with maximum vertical velocity (wmax) between 10 and 12 m s^{-1}, and the frequency drops off sharply with increasing wmax. There are 23 sondes that sampled vertical velocities in excess of 15 m s^{-1}, and 6 that sampled vertical velocities in excess of 20 m s^{-1}. These magnitudes are comparable to the strongest updrafts that have been observed in any tropical cyclone from flight-level and Doppler radar data, though most of the extreme updrafts from these prior studies were sampled at heights above 3 km (Jorgensen et al. 1985; Black et al. 1994, 1996; Guimond et al. 2010; Heymsfield et al. 2010). Figure 3d shows the histogram of maximum horizontal wind speed for the ws90 sondes. As with the extreme updrafts, the frequency of extreme wind speeds drops off sharply with increasing magnitude, though there are 19 sondes with

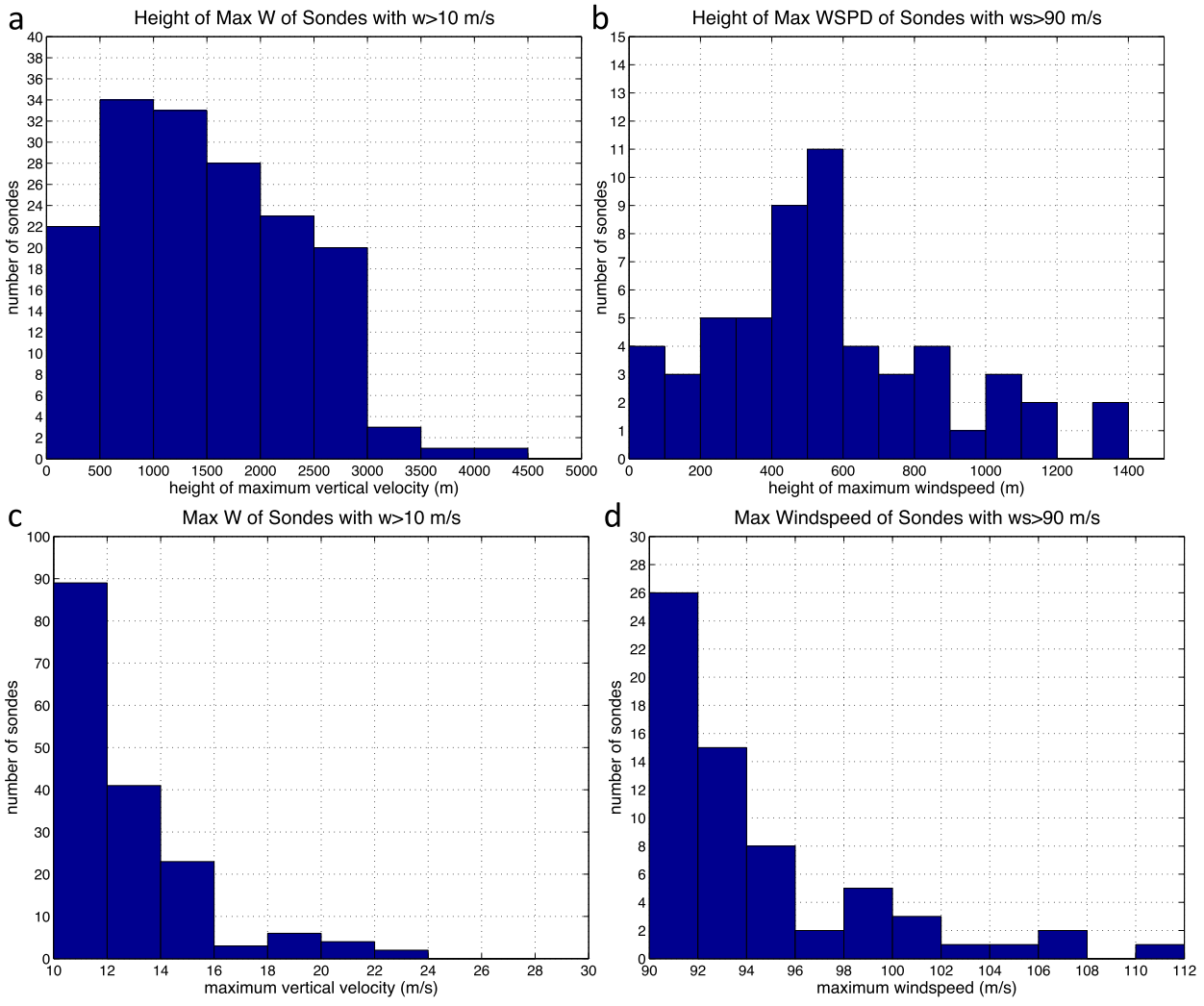

FIG. 3. Histograms of the heights (m) of maximum vertical velocity and horizontal wind speed for the (a) w10 and (b) ws90 datasets, respectively. Histograms of the maximum vertical velocity and horizontal wind speed for the (c) w10 and (d) ws90 datasets, respectively. For (a) and (b), 165/169 and 56/64 sondes are shown, respectively. For (c) and (d), 168/169 and 64/64 sondes are shown, respectively. Note that the *x*-axis range and bin size are different between (a) and (b).

wind speeds exceeding $95\,m\,s^{-1}$, and 8 exceeding $100\,m\,s^{-1}$. There is no apparent relationship between the heights of maximum vertical and horizontal velocities and their respective magnitudes (Fig. 4). For w10, this lack of relationship suggests that buoyancy is unlikely to be important as a forcing for these low-level updrafts, which we discuss further in section 5.

b. Radial location of sondes relative to the RMW

Most previous observational studies have found that the strongest updrafts in tropical cyclones are within the eyewall. For example, Black et al. (1994) found that for Hurricane Emily (1987): "all of the extreme vertical velocity events occurred in the eyewall" (p. 2723). However, in some studies the strongest updrafts in rainbands were only slightly weaker than those in the eyewall (Jorgensen et al. 1985). In our preliminary investigation, Stern and Aberson (2006) found that the upsondes were almost exclusively found within the eyewall, and based on the sonde profiles, appeared to often be at the inner edge of the eyewall. To more conclusively determine the region where these sondes are found, we compare the location of the sondes to the flight-level radius of maximum winds. Recently, Vigh et al. (2016) assembled a dataset of all NOAA and USAF flight-level data from 1997 to 2013. In this dataset, termed FLIGHT+, the endpoints of individual radial legs have been determined, and the distance of the plane to the storm center has been computed. Utilizing the FLIGHT+ dataset, we have matched the drop time of each sonde to the flight-level

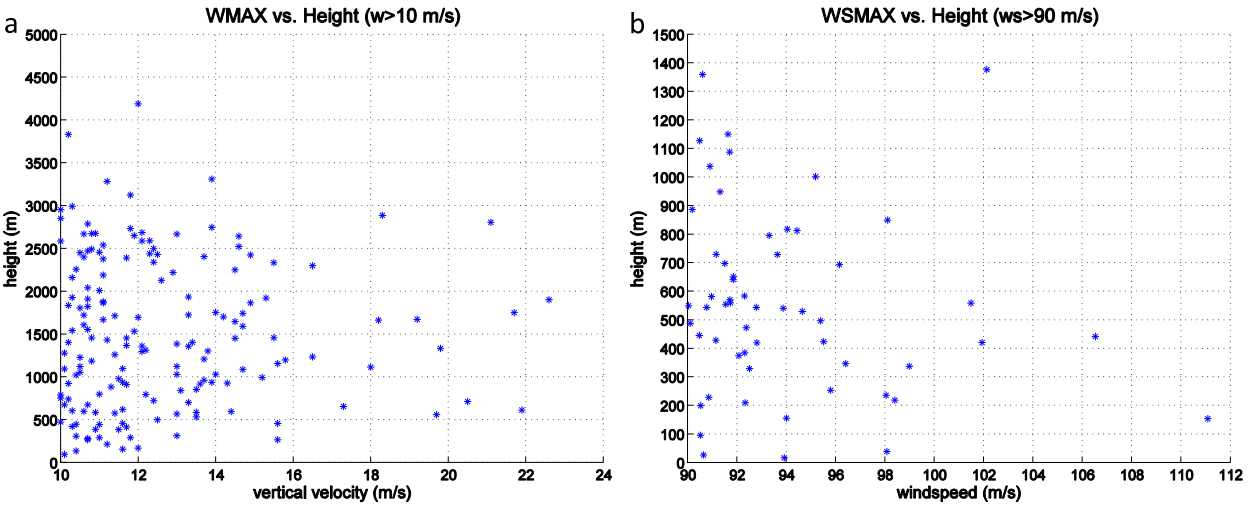

FIG. 4. (a) Maximum vertical velocity and (b) horizontal wind speed vs height for the w10 and ws90 datasets, respectively. For (a) and (b), 165/169 and 56/64 sondes are shown, respectively. Note that the *y*-axis range is different between (a) and (b).

data, and found the RMW from the respective flight leg. To calculate the distance from the center, FLIGHT+ uses the "trak" files produced by HRD, which give storm center latitude and longitude every 2 min in time, based on the method of Willoughby and Chelmow (1982). We also use the trak files to compute the distance of each sonde from the (time varying) storm center at all points along its trajectory.

Figure 5a illustrates the location of flight-level maximum winds for each w10 sonde (blue dots), the location where each sonde was dropped (black dots), and the location of maximum sonde vertical velocity (red dots). Most sondes were dropped within 40 km of the storm center, indicating that they were within the inner core region. Within this region, there is no apparent preference for radius. This is because of variations in RMW among the storms in the dataset, as demonstrated by Fig. 5b, which shows the radius of sonde maximum vertical velocity versus flight-level RMW. Figure 5b indicates that most of the extreme updrafts are found very close to (but slightly inward of) the flight-level RMW, and are therefore within the eyewall. Nearly 90% of the sondes were dropped between 0 and 10 km inside of the flight-level RMW, with a median of about 3 km inside of the RMW. Figure 5c is the same as Fig. 5a, but with the radius shown relative to the flight-level RMW. There is no obvious systematic relationship between the height of the maximum updraft and the radius relative to the RMW, though this result may be a consequence of limited sampling.

Figure 6 is similar to Fig. 5, but for the ws90 sondes. All of the extreme wind speeds are found within 50 km of the storm center (Fig. 6a). This is simply a reflection of the fact that the RMW for all such cases is smaller than 50 km (Fig. 6a), as wind speeds in excess of 90 m s^{-1} are only found near the RMW (Fig. 6b), and only in the most intense tropical cyclones, which tend to have relatively small RMWs (Kimball and Mulekar 2004; Stern et al. 2015). Almost all ws90 sondes were dropped between 0 and 10 km inside of the flight-level RMW, with the median drop location 4 km inside of the RMW. Although the height of peak sonde wind speed increases with radius (Fig. 6a) and with flight-level RMW (not shown), there does not appear to be any systematic relationship between the radius of the sonde *relative* to the RMW and the height of maximum wind speed (Fig. 6c). As with the w10 sondes however, we cannot preclude the possibility that this lack of relationship is a consequence of limited and/or biased sampling.

The patterns seen in Figs. 5 and 6 are likely explained in part by standard mission protocol. The USAF reconnaissance missions are generally mandated to drop eyewall sondes just inward of the flight-level RMW and so, by design, there are relatively few sondes that sample the region just outside of the flight-level RMW. NOAA research missions tend to drop more sondes and are also much more variable in sonde location, with occasional missions dropping numerous sondes across the eyewall. Nevertheless, on average, NOAA also tends to drop preferentially just inside of the flight-level RMW. Both USAF and NOAA will drop sondes in rainbands or in regions well outside of the eyewall. However, the sonde coverage is, in general, much sparser outside of the eyewall region. Despite this major caveat, the dropsonde observations strongly suggest that extreme low-level updrafts in tropical cyclones are nearly exclusively found in the eyewall region.

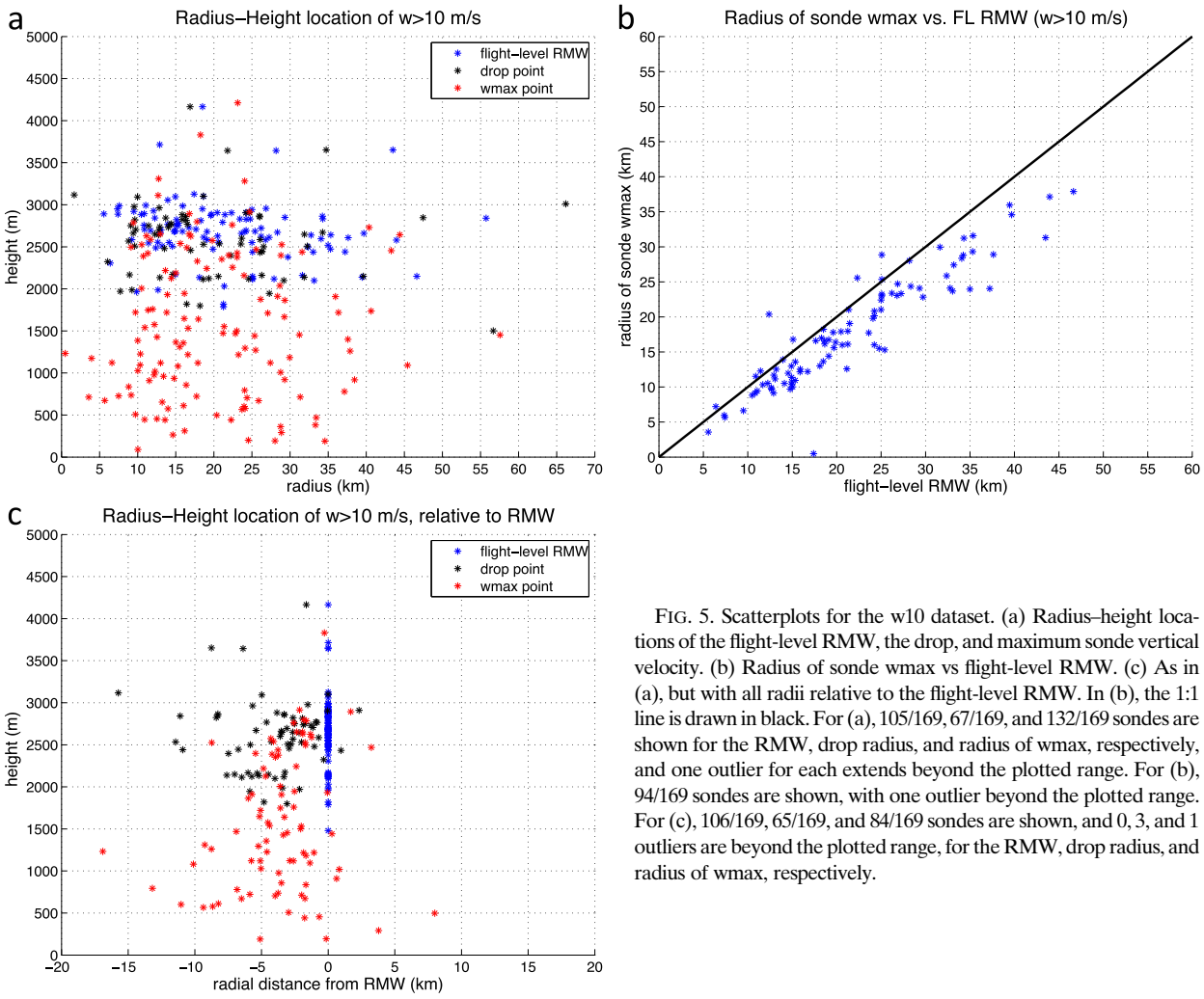

FIG. 5. Scatterplots for the w10 dataset. (a) Radius–height locations of the flight-level RMW, the drop, and maximum sonde vertical velocity. (b) Radius of sonde wmax vs flight-level RMW. (c) As in (a), but with all radii relative to the flight-level RMW. In (b), the 1:1 line is drawn in black. For (a), 105/169, 67/169, and 132/169 sondes are shown for the RMW, drop radius, and radius of wmax, respectively, and one outlier for each extends beyond the plotted range. For (b), 94/169 sondes are shown, with one outlier beyond the plotted range. For (c), 106/169, 65/169, and 84/169 sondes are shown, and 0, 3, and 1 outliers are beyond the plotted range, for the RMW, drop radius, and radius of wmax, respectively.

c. *Azimuthal distribution of extreme updrafts and horizontal wind speeds*

Figure 7a shows the storm-relative horizontal location of the maximum vertical velocity for the w10 sondes, and Fig. 8a shows the storm-relative location of the maximum wind speed for the ws90 sondes. For w10, most of the sondes are found between northeast and west of the storm center (going counterclockwise). This general left-of-center bias is less evident in the ws90 sondes than in the w10 sondes, possibly due to the smaller sample size. Nevertheless, the peak in the distribution is west of center for both datasets, and few sondes are found in the southern semicircle. Figures 7b and 8b show the location of the w10 and ws90 sondes, but with the azimuth relative to the direction of storm motion. Figures 7c and 8c show the location of the w10 and ws90 sondes, but with the azimuth relative to the direction of the deep layer (200–850 hPa) environmental vertical wind shear vector. Figures 7d–f and 8d–f show histograms of the azimuthal locations for the w10 and ws90 sondes, respectively. We calculate storm motion from HRD trak files, and we obtain the deep-layer shear from the Statistical Hurricane Intensity Prediction Scheme (SHIPS) dataset (DeMaria et al. 2005).

For the w10 sondes, there is a broad maximum in motion-relative azimuth (Figs. 7b,e) between 30° to the left and 90° to the right of storm motion (58%; 83 of the 144 w10 sondes with location data). Relative to shear (Figs. 7c,f), there is a strong tendency for the maximum vertical velocity of the w10 sondes to be in the left-of-shear semicircle (77%; 111/144), with the peak of the distribution 90°–120° to the left of shear (i.e., slightly toward the upshear-left quadrant). A slightly larger fraction of the sondes are found in the upshear-left quadrant (42%; 60/144) than in the downshear-left quadrant (35%; 51/144).

For the ws90 sondes, the azimuthal distribution is quite similar as that of the w10 sondes. Relative to storm

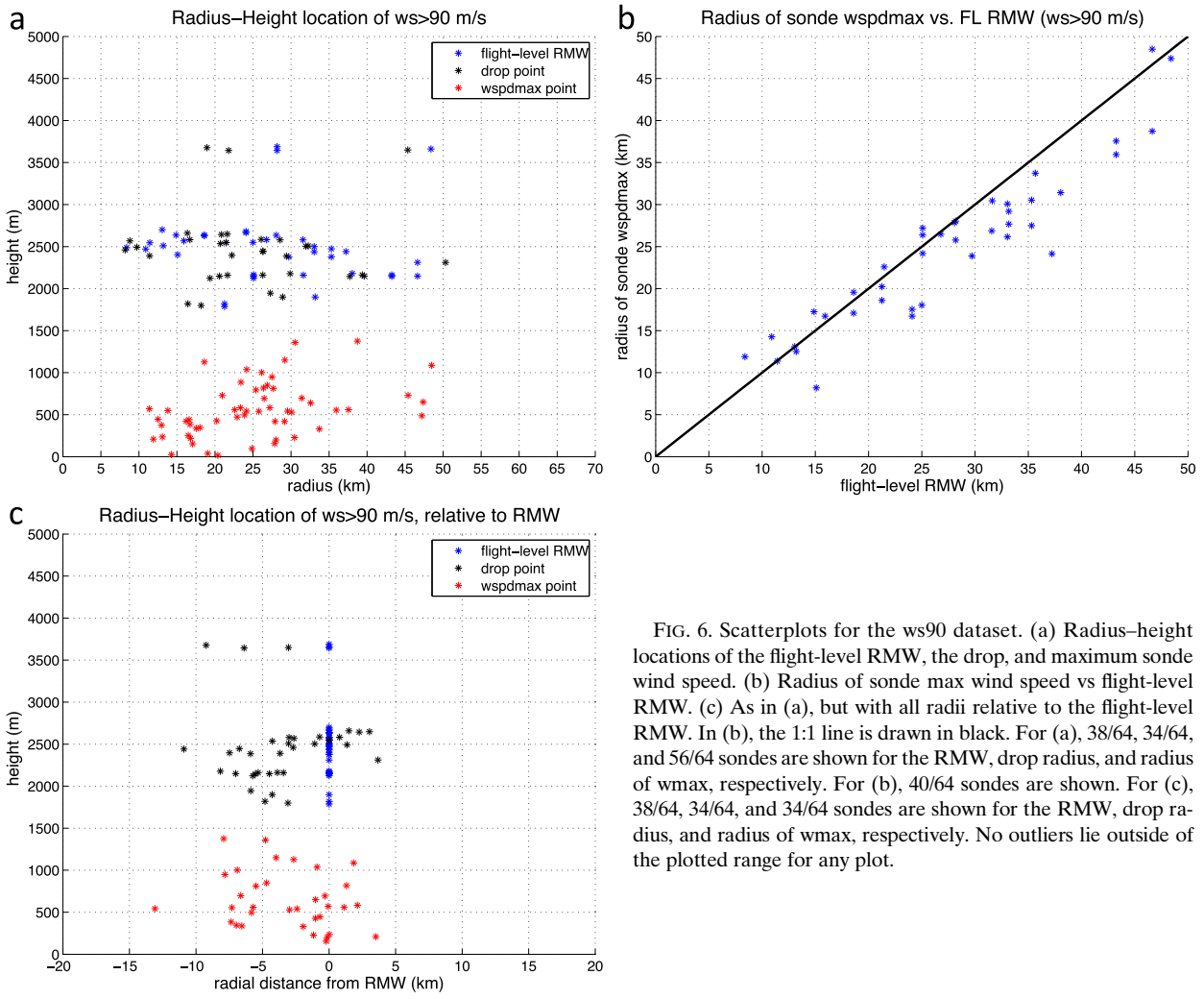

FIG. 6. Scatterplots for the ws90 dataset. (a) Radius–height locations of the flight-level RMW, the drop, and maximum sonde wind speed. (b) Radius of sonde max wind speed vs flight-level RMW. (c) As in (a), but with all radii relative to the flight-level RMW. In (b), the 1:1 line is drawn in black. For (a), 38/64, 34/64, and 56/64 sondes are shown for the RMW, drop radius, and radius of wmax, respectively. For (b), 40/64 sondes are shown. For (c), 38/64, 34/64, and 34/64 sondes are shown for the RMW, drop radius, and radius of wmax, respectively. No outliers lie outside of the plotted range for any plot.

motion (Figs. 8b,e), there is a tendency for the ws90 sondes to be found in the right-front quadrant (44%; 28/64), similar to the w10 sondes (44%; 63/144). As with the w10 sondes, the shear-relative distribution of ws90 sondes peaks 90°–120° to the left of shear (Figs. 8c,f), and there is a clear dominance of the left-of-shear semicircle (84%; 54/64). The greatest frequency is in the upshear-left quadrant (48%; 31/64), with a slightly smaller fraction in the downshear-left quadrant (36%; 23/64). Although a substantial fraction of the ws90 sondes are also w10 sondes, the above relationships between the location of maximum wind speed in the ws90 sondes and the directions of storm motion and vertical wind shear remain the same when the overlapping sondes are excluded (not shown).

Figures 9a and 9b show the maximum updrafts in the w10 dataset as a function of storm translation speed and vertical wind shear magnitude, respectively. Figures 9c and 9d show analogous plots for the maximum wind speeds in the ws90 dataset. The w10 dataset includes cases with a wide range of both storm translation speed (1.3–23.9 kt) and vertical wind shear magnitude (1.4–39.2 kt), though most cases fall between 5 and 20 kt for both. The ws90 dataset also spans a wide range of both storm translation speed (3.5–27.4 kt) and vertical wind shear magnitude (3.2–22.0 kt), though the maximum analyzed shear is substantially less than for w10. This difference is to be expected, as vertical wind shear generally acts to weaken tropical cyclone intensity. Also, while the datasets span similar ranges of translation speed, most ws90 sondes occur with storm speeds of between 6 and 13 kt, while the storm speeds for the w10 sondes are more widely scattered. There is no apparent relationship between either the storm speed or shear magnitude and the maximum updraft in w10 or the maximum wind speed in ws90. For w10, this is evidence that although shear systematically organizes the azimuthal location of the extreme updrafts, the magnitude

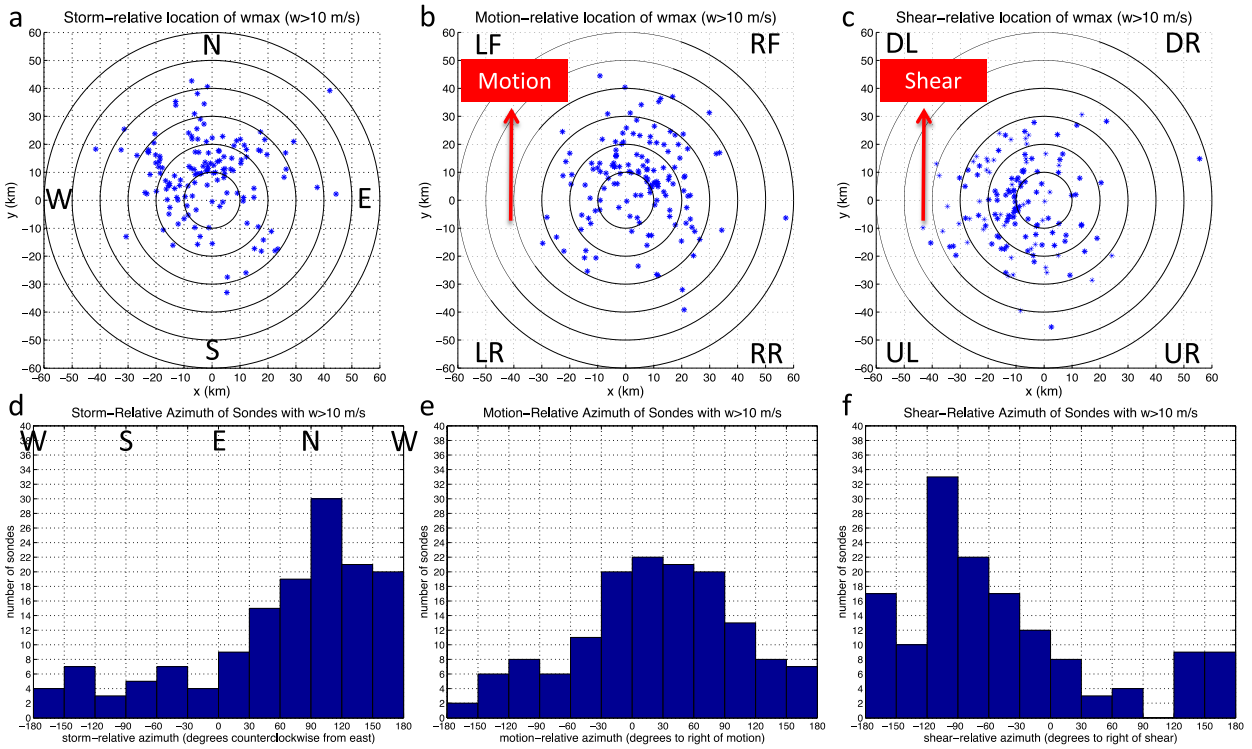

FIG. 7. For the w10 sondes, the horizontal location of the maximum vertical velocity, relative to (a) the storm center, (b) storm motion vector, and (c) environmental wind shear vector. (d)–(f) As in (a)–(c), but for histograms of the azimuth of maximum vertical velocity. Cardinal directions are indicated in (a) and (d), the left-front (LF), right-front (RF), left-rear (LR), and right-rear (RR) quadrants are indicated in (b), and the downshear-left (DL), downshear-right (DR), upshear-left (UL), and upshear-right (UR) quadrants are indicated in (c). For (a)–(c), range rings are drawn in black every 10 km. For (a)–(c), 143/169 sondes are shown, while for (d)–(f), 144/169 sondes are shown. Note that one sonde whose location is beyond the plotted range is not shown for (a)–(c).

of the shear does not seem to significantly modulate the intensity of these updrafts. This suggests that deep layer environmental vertical wind shear might not actually be a contributor to the existence of these updrafts, but instead may serve to suppress extreme updrafts in the right-of-shear quadrants, that would otherwise occur in the absence of shear.

Given the strong apparent relationships between the azimuthal distribution of the w10 (and ws90) sondes and both the storm motion and shear headings, it is likely that there is also a relationship between the storm motion and the shear headings. Indeed, there is such a relationship: for greater than half the cases in our dataset, the motion vector is between 90° and 180° to the left of the shear vector (not shown). This same issue was addressed by Corbosiero and Molinari (2003, hereafter CM03), who examined the relationships between lightning strike location (a proxy for convection), storm motion, and vertical wind shear. We use the methods outlined in CM03 to examine whether environmental vertical shear or storm motion has a greater influence on the azimuthal distribution of w10 sondes. Figure 10 shows that for motion opposite to shear or motion to the left of shear (where the favorable regions for motion and shear are largely aligned), the strong front quadrant preference seen in the full dataset remains. In contrast, for motion in the same direction as shear or motion to the right of shear, there is no preference of azimuth. Taken together, these results indicate that the effect of shear on modulating the azimuthal distribution of extreme updrafts is dominant over that of storm motion, which is consistent with CM03.

At the suggestion of a reviewer, we examined the possibility that asymmetric sampling may influence the apparent distribution of the w10 and ws90 sondes relative to the environmental vertical shear. Indeed, Wang et al. (2015) recently showed (see their Fig. 5) that the combined distribution of all NOAA P3 and GIV sondes are quite azimuthally asymmetric, with about twice as many sondes dropped to the north of TCs as to the south. To assess the effect of asymmetric sampling on our results, we acquired the Wang et al. (2015) dataset and examined only P3 sondes, as we do not consider GIV sondes in our datasets. The overall distribution of P3 sondes is substantially more symmetric than that of the combined dataset presented in Wang et al. (2015). Nevertheless, there are about 45% more sondes to the

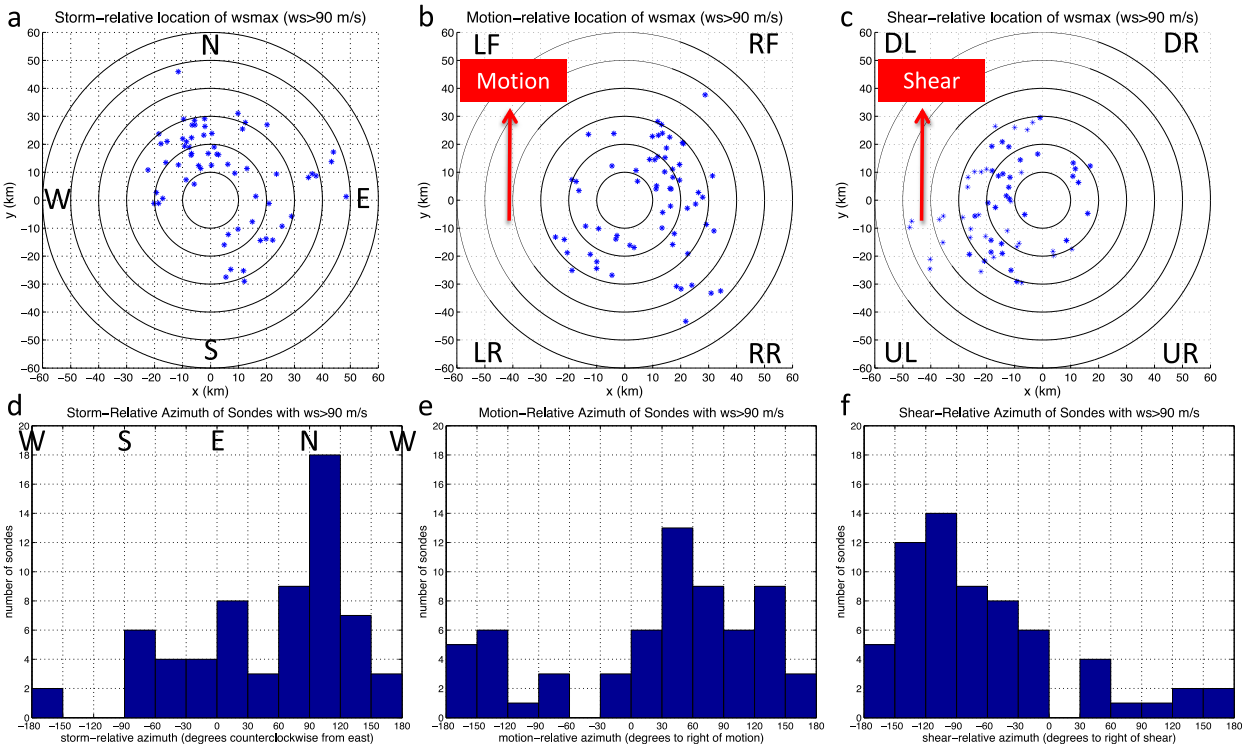

FIG. 8. (a)–(f) As in Fig. 7, but for the ws90 sondes; 64/64 sondes are shown.

north than to the south (not shown). We then matched the inner-core ($r \leq 100$ km) P3 sondes in the Wang et al. (2015) dataset to the SHIPS shear dataset, and there is a shear-relative asymmetry in sampling as well. However, by calculating the distribution of vertical velocity, binned by the shear-relative azimuth to remove the effect of asymmetric sampling, we can determine the relationship between the distribution of strong updrafts and the shear orientation. For the 95th percentile, w is nearly twice as large to the left of shear as compared to the right of shear (not shown). This result establishes that there is a strong relationship between updraft strength and shear-relative location across all sondes, irrespective of sampling bias. This further implies that what we showed in Figs. 7 and 8 is robust; there is a strong preference for extreme updrafts and wind speeds to be found left of shear. Finally, note that the Wang et al. (2015) dataset does not contain any USAF sondes, whereas our datasets do. The USAF drops are expected to be largely symmetric, and so this further mitigates any effect of asymmetric sampling from the NOAA P3 sondes.

5. Are the extreme updrafts driven by buoyancy?

Several studies (Zhang et al. 2000; Braun 2002; Smith et al. 2005; Eastin et al. 2005a,b, hereafter E05a and E05b, respectively) have investigated whether or not eyewall updrafts are substantially buoyant, and/or whether buoyancy is the predominant source of vertical acceleration for the updrafts. E05a,b utilized flight-level temperature and vertical velocity data from 175 radial legs (ranging from 1.5- to 5.5-km height) in 14 intense hurricanes in order to assess the buoyancy of updrafts. E05a,b calculated the thermal buoyancy as

$$\mathrm{TB} = g\frac{\theta_v'}{\overline{\theta}}, \tag{2}$$

where $\overline{\theta}$ and θ_v' are the mean potential temperature and perturbation virtual potential temperature, respectively. E05a,b defined the mean to be the value after application of a 20-km low-pass filter, and the perturbation to be the deviation of the total value from the filtered time series. The strongest updraft in their dataset was 16.0 m s^{-1}, at 4.2-km height. Most updraft cores were much weaker, however, just 1 or 2 m s^{-1}. Total buoyancy (in terms of temperature perturbations) ranged from −1.9 to 1.7 K, with a median of 0.16 K. As the updraft magnitude increased somewhat with height within their dataset, E05a,b suggested that buoyancy is likely responsible for vertical accelerations between low- and midlevels. As we will discuss, the updrafts examined by E05a,b were, on average, sampled at substantially higher altitudes than those in our dataset, and this is a critical distinction.

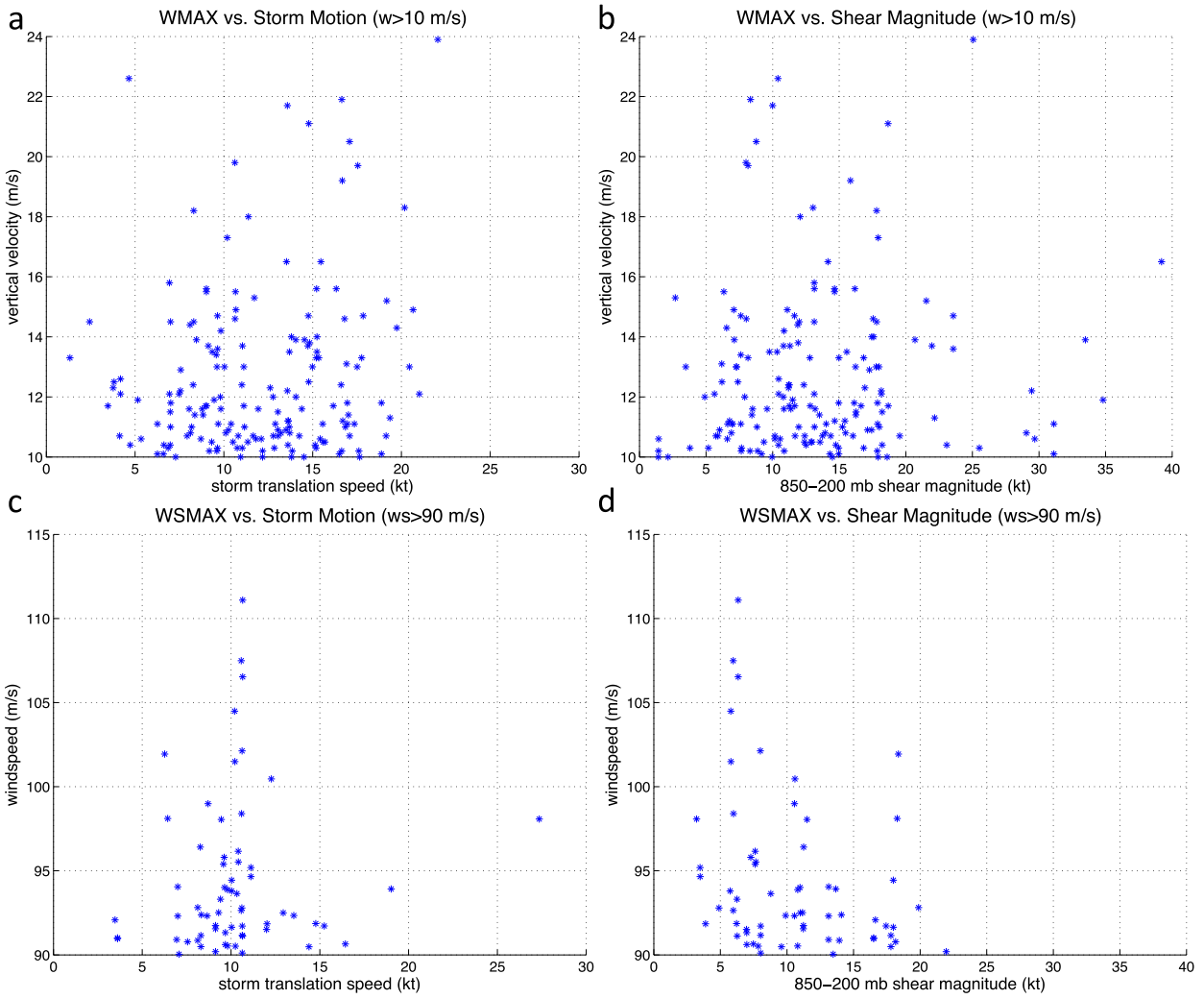

FIG. 9. For the w10 sondes, (a) maximum vertical velocity ($m\,s^{-1}$) vs the storm translation speed (kt) and (b) the magnitude of the environmental wind shear (kt). (c),(d) As in (a),(b), but for the maximum wind speed ($m\,s^{-1}$) for the ws90 sondes. For (a),(b), 168/169 sondes are shown, while for (c),(d), 64/64 sondes are shown.

E05a,b then used a one-dimensional updraft model to calculate the median updraft at different flight levels:

$$\frac{dw}{dz} = \frac{1}{w}\left(\frac{1}{\rho}\frac{\partial p'}{\partial z} + B\right), \tag{3}$$

where p' is the perturbation pressure, and B is the total buoyancy (defined as the sum of thermal buoyancy, dynamic buoyancy, and water loading; the latter two of which E05a,b found to be relatively small). Because there was no way to determine the perturbation vertical pressure gradient force, E05a,b only calculated the acceleration from buoyancy. They found that the predicted median updrafts from (3) at the levels above 1.5 km were much greater than the actual median updraft velocities (about 5.5 $m\,s^{-1}$ predicted vs 1.5 $m\,s^{-1}$ observed, at 5.5-km height). From this, E05a,b concluded that buoyancy was "the primary force vertically accelerating the eyewall and rainband updraft cores above the boundary layer" (p. 203 of E05a). Note that in this updraft model, it is implicitly assumed that the eyewall convection is deep and vertically coherent through at least the 1.5–5.5-km layer.

We will not attempt to quantitatively estimate buoyancy from the w10 dropsonde dataset, for several reasons. First, a dropsonde trajectory in the eyewall of a major hurricane is much closer to horizontal than to vertical, and it is unlikely that the sounding well beneath a given updraft maximum is representative of the air that enters the updraft. More importantly, it is impossible to determine the perturbation vertical

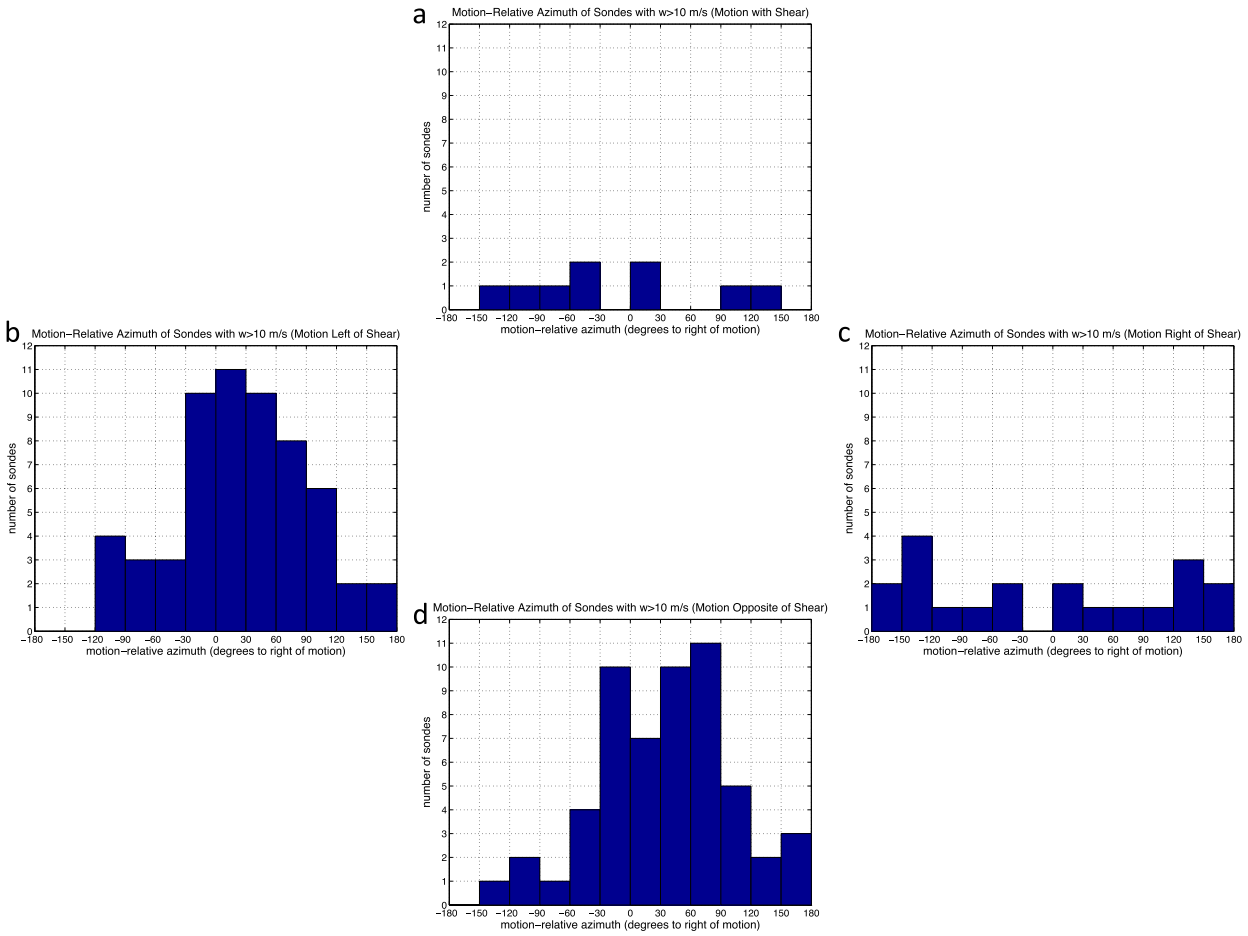

FIG. 10. As in Fig. 7e, but subdivided into those w10 sondes where (a) the motion and shear headings are aligned, (b) motion is to the left of shear, (c) motion is to the right of shear, and (d) the motion and shear headings are opposed. For each panel, sondes are included that are within ±45° of the respective orientation. A total of 144/169 sondes are shown in (a)–(d).

pressure gradient force from this dataset. The thermal buoyancy is strongly dependent on a somewhat arbitrary reference state, and so it is not particularly meaningful to examine the buoyancy term on its own (Doswell and Markowski 2004). Nevertheless, we can use the same updraft model as E05a,b in order to demonstrate that it is highly implausible that the extreme low-level updrafts (below 1.5 km) in the w10 dataset are driven by buoyancy.

Figures 11 and 12 show the vertical profiles of vertical velocity and temperature, respectively, for the four strongest updrafts whose wmax is found below 1000 m. Each of these has vertical velocity exceeding 17 m s^{-1}, at heights between 500 and 800 m. If we assume that buoyancy is constant with height between the surface and the height of maximum updraft, and we neglect the perturbation pressure gradient force, then we can solve for the value of B necessary to produce an updraft of a given magnitude at a given height:

$$B = \frac{w^2}{2\Delta z}, \tag{4}$$

where Δz is the depth over which a parcel accelerates. If we conservatively take Δz to be 800 m and w to be 17 m s^{-1}, this yields a required buoyancy of 0.1806 m s^{-2}. Assuming a value of 300 K for $\overline{\theta}$, (2) yields a virtual potential temperature perturbation of 5.5 K. Such a perturbation is extremely large, and would be clearly evident on a sounding if such a perturbation existed. Figure 12 indicates that none of these sondes exhibit such perturbations. There are 11 w10 sondes where wmax is found below 350 m. Using w of 12 m s^{-1} and Δz of 300 m, the required temperature perturbation is 7.3 K. This magnitude perturbation is implausible, and is not evident in any of the temperature profiles (not shown). Note that these are almost certainly underestimates of the required perturbations, as buoyancy is unlikely to be

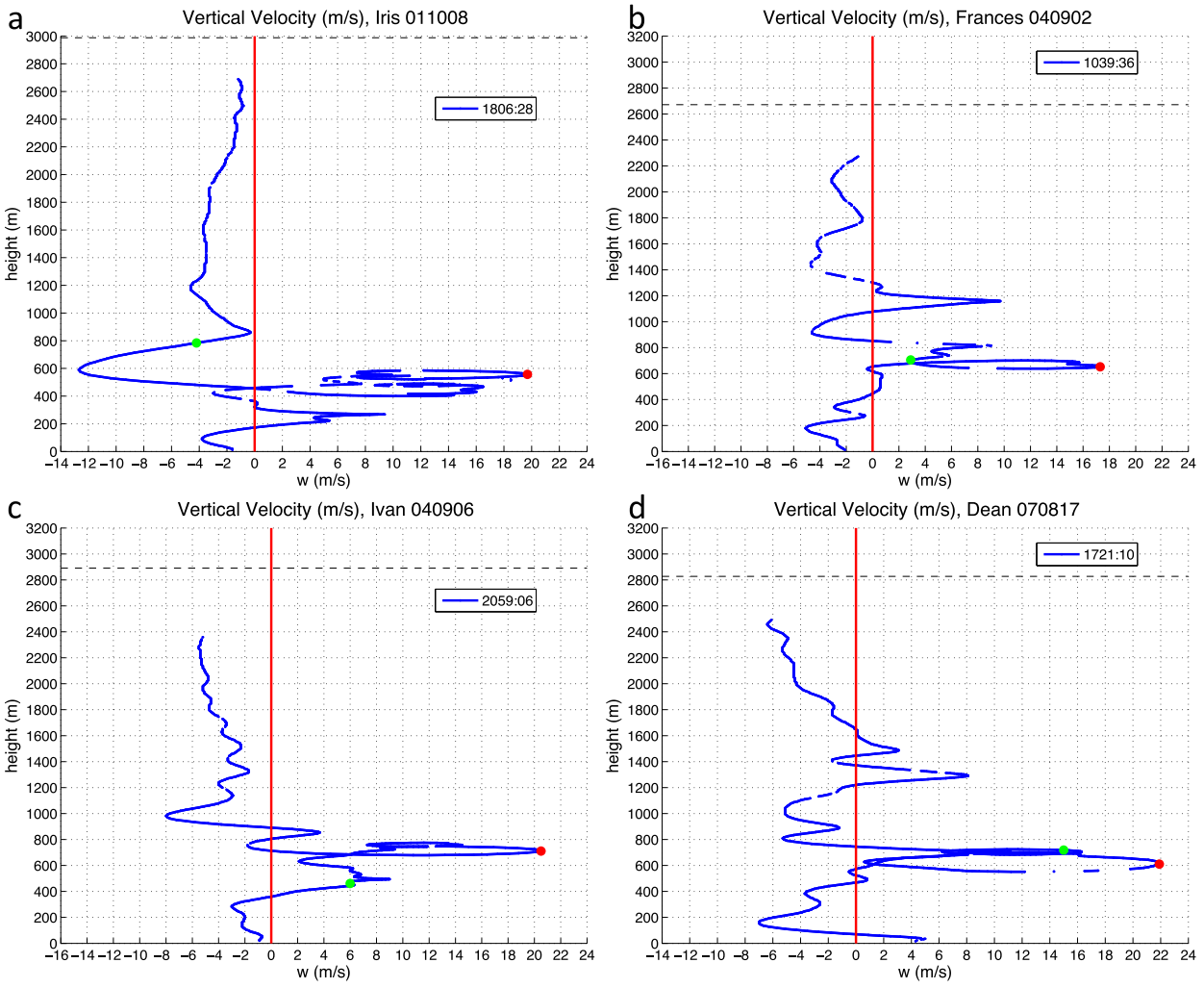

FIG. 11. Vertical profiles of vertical velocity for the four sondes with the strongest updraft maximum that is found below 1000-m height. The storm name and date are given in the titles, and the drop time is given in the legends. The flight-level altitude is indicated by the dashed horizontal line. The red vertical line indicates $w = 0\,\mathrm{m\,s^{-1}}$. The red and green filled circles indicate the point of maximum vertical velocity and horizontal wind speed, respectively. Note that both the x and y range are not identical between panels. Also note that each of these sondes experience periods of rising, and so the vertical velocity is multivalued at some heights.

constant with height (an assumption that minimizes the required perturbation), and the perturbation vertical pressure gradient force that is associated with thermal buoyancy generally opposes thermal buoyancy (Doswell and Markowski 2004). In order for buoyancy to be responsible for the vertical accelerations that produce these updrafts, the temperature perturbation must be even greater than these already large estimates. This is implausible, and so buoyancy cannot be the primary driver of these extreme low-level updrafts.

There are likely several reasons for the differences between our results and those of E05a,b. First, while there were a few updrafts included in E05a,b that were similar in strength to those in our dataset, most of the updrafts examined by E05a,b were much weaker, only 1 or $2\,\mathrm{m\,s^{-1}}$. Therefore, the required temperature perturbations for buoyancy to drive the updrafts in E05a,b are much less than for our dataset. For our simple example in (4), a buoyantly driven $10\,\mathrm{m\,s^{-1}}$ updraft requires 100 times the temperature perturbation of a $1\,\mathrm{m\,s^{-1}}$ updraft, assuming that the acceleration occurs over the same depth. Second, while E05a,b did examine data as low as 1.5 km, the average height of the updrafts in their study was substantially higher than those in our dataset. This is important, as the greater the height of a given updraft, the lesser the required temperature perturbation, assuming buoyancy as the driving force. For constant buoyancy, vertical velocity will increase with

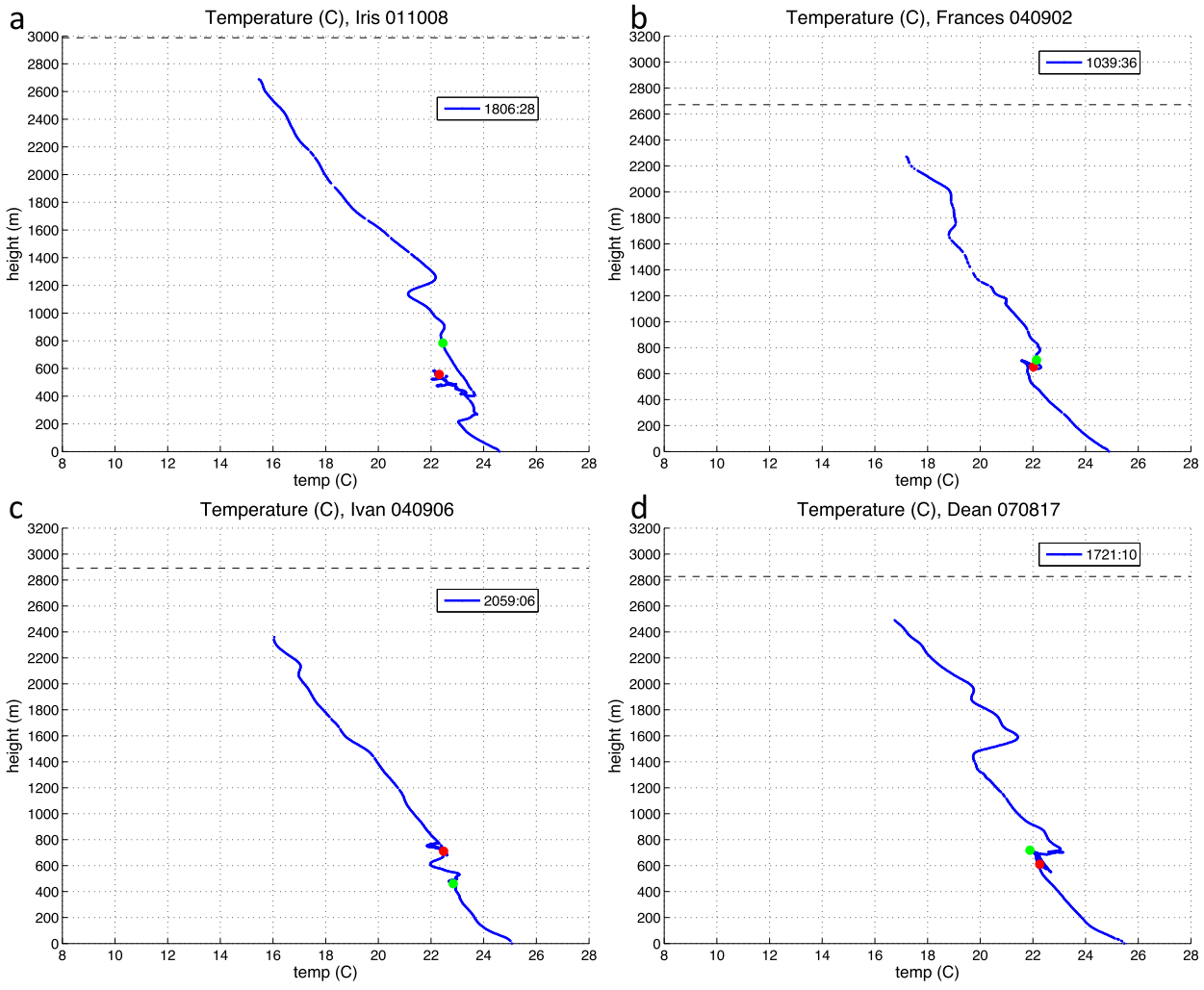

FIG. 12. As in Fig. 11, but for vertical profiles of temperature.

the square root of the depth of parcel displacement. Alternatively, this means that the required buoyancy for a given updraft is inversely proportional to the depth. Assuming a parcel originating at the surface in the presence of a constant buoyancy forcing, a $10\,m\,s^{-1}$ updraft at 5-km height only needs a temperature perturbation 20% of that for a $10\,m\,s^{-1}$ updraft at 1-km height. These two factors can largely explain why the relatively modest temperature perturbations found by E05a,b can plausibly be responsible for the updrafts in their dataset, whereas such temperature perturbations cannot plausibly be responsible for the updrafts in our dataset. Therefore, our results are not necessarily contradictory to those of E05a,b, but instead may support E05a,b, by clarifying the importance of the depth of forcing in determining whether buoyancy is a primary contributor to updraft acceleration.

6. Other characteristics of extreme updrafts and horizontal wind speeds

a. *Sondes that sample intense vortices along the edge of the eyewall?*

Of the 64 ws90 sondes, 24 (38%) also sample updrafts greater or equal to $10\,m\,s^{-1}$, and so are included in both datasets. This overlap suggests that there might be some physical relationship between extreme updrafts and extreme horizontal wind speeds. Examining all such sondes, however, we found no obvious general correspondence in structure between the profiles of horizontal wind speed and vertical velocity. For some of these sondes, the maximum updraft is found much higher (1–2 km) than the maximum wind speed, and with no strong updraft found close by (in time) to the wind speed maximum. There are some sondes, however,

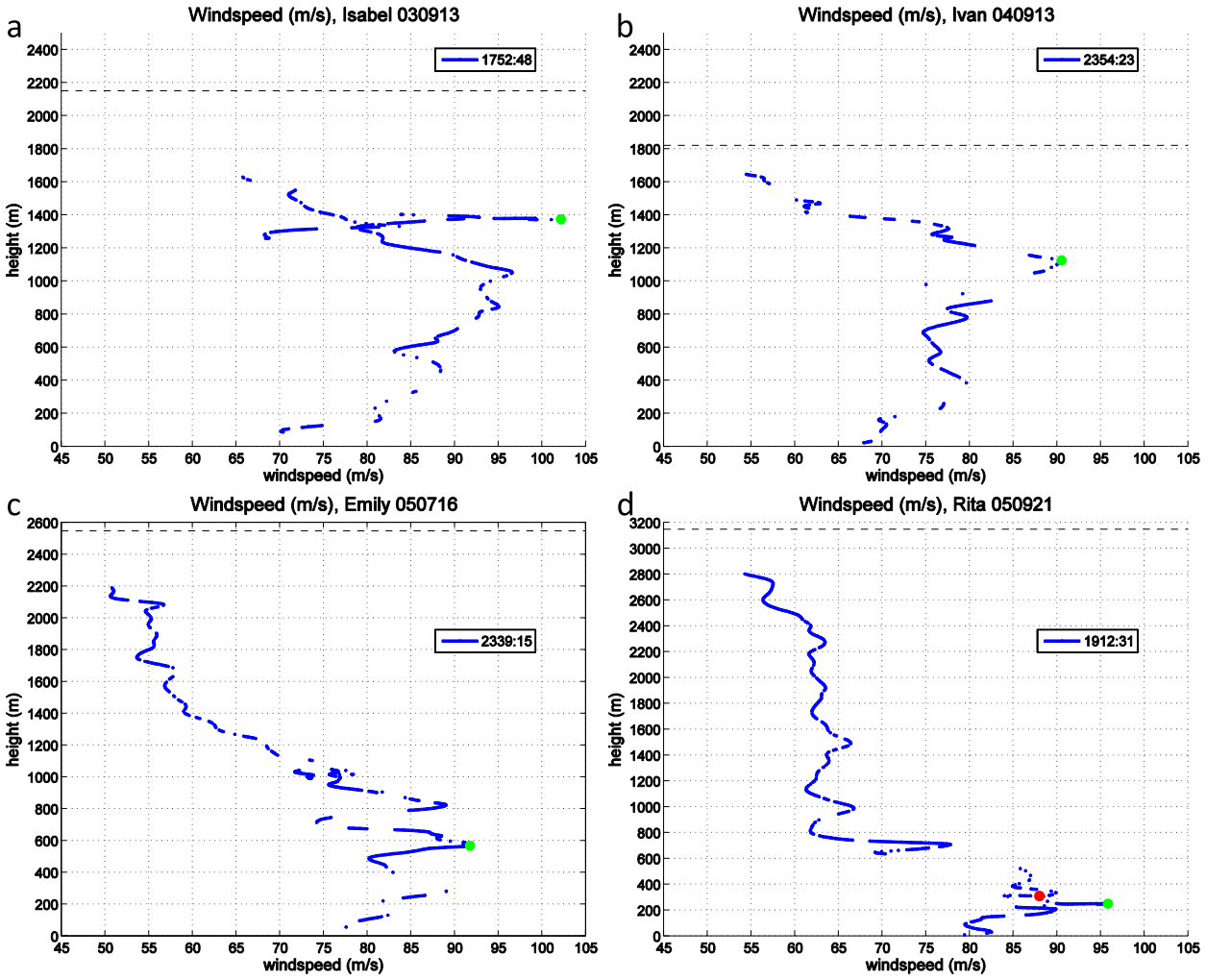

FIG. 13. Vertical profiles of wind speed for four sondes that are members of both datasets and where the maximum vertical velocity is found relatively near to the maximum wind speed. The storm name and date are given in the titles, and the drop time is given in the legends. The flight-level altitude is indicated by the dashed horizontal line. The red and green filled circles indicate the point of maximum vertical velocity (missing in some cases because of missing height data at time of maximum) and horizontal wind speed, respectively.

where the maxima are found relatively close to one another, within a couple hundred meters. Figure 13 shows the profiles of wind speed and Fig. 14 shows vertical velocity, for four sondes that are members of both datasets. As discussed in Aberson et al. (2006), the Isabel sonde exhibits very large fluctuations in horizontal wind speed during the time of the extreme updraft, varying by about 35 m s^{-1} while the sonde was at approximately constant height. The fact that such variability in wind speed is coincident with the updraft implies that these two characteristics may be linked. At the time of maximum wind speed, the vertical velocity is 10.5 m s^{-1}, and this represents the greatest such value among the ws90 sondes (not shown). Aberson et al. (2006) presented additional observational evidence that the sonde likely was dropped into a small scale vortex on the inner edge of the eyewall. Based on the qualitative similarity between this sonde and other sondes within our datasets (e.g., Figs. 13–14), we believe that a number of such sondes may be sampling intense vortices on the edge of the eyewall.

The Emily and Rita sondes also have vertical velocities of about 10 m s^{-1} at the time of maximum horizontal wind speed, while the Ivan sonde is about 5 m s^{-1}. These other three sondes also exhibit large fluctuations in wind speed, although not quite as great as in the Isabel sonde. The fluctuations in vertical velocity sometimes appear to be in phase with those of wind speed, whereas at other times they are not, which can be seen more readily in time series plots (Fig. 15). There is variation on different

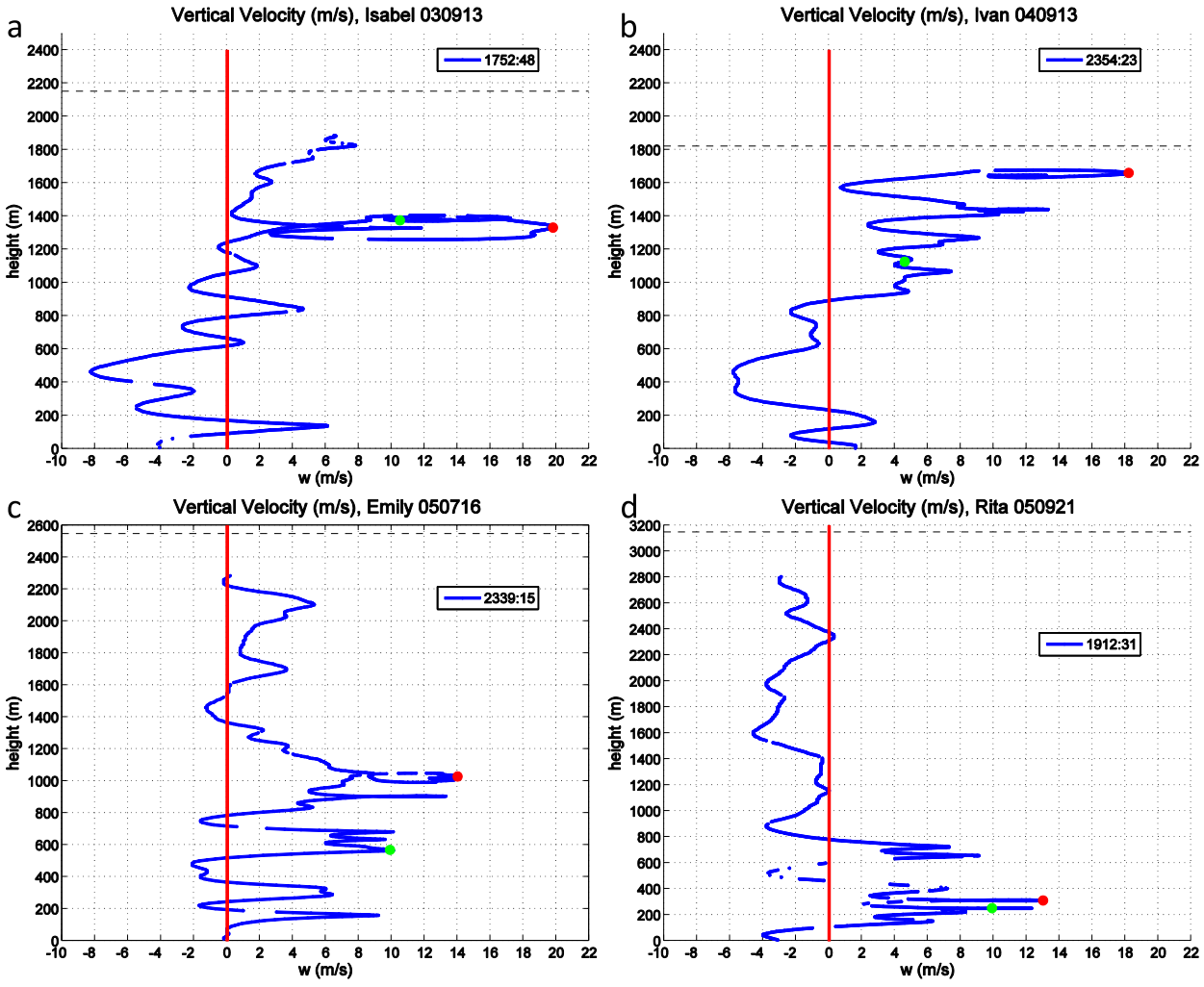

FIG. 14. As in Fig. 13, but for vertical velocity.

time scales, and it appears that the vertical velocity is somewhat more variable than the wind speed. It is therefore difficult to more precisely define the relationship between the two fields, from dropsonde observations alone.

b. Multiple nearby sondes sampling extreme updrafts

Occasionally, NOAA flights will release consecutive sondes at very short intervals, allowing for sampling at relatively high radial resolution. As a result, sometimes two or more sondes will sample extreme updrafts within the same azimuthal portion of the eyewall at nearly the same time. For the w10 dataset, there are nine sets of (at least) two consecutive sondes dropped with less than 40 s (about 5 km) intervals between sondes. For the ws90 dataset, there are 10 such sets of sondes. Even though these sondes were dropped within a few kilometers of each other, in most cases it is unlikely that they sampled the same feature (Marks et al. 2008; Aberson et al. 2006). Nevertheless, we can learn something about the structure and frequency of these updrafts by examining these multisonde sequences. Note that there are other sondes within the datasets that were dropped as part of a sequence, but where the remaining sondes within the sequence did not sample either $10\,\mathrm{m\,s^{-1}}$ updrafts or $90\,\mathrm{m\,s^{-1}}$ wind speeds. For example, there are 29 such sequences that only include a single w10 sonde. From the fact that almost a quarter (9/38) of these multisonde sequences contain more than one w10 sonde, we can infer that for storms that do possess such strong low-level updrafts, these updrafts are not rare. Further, although a single eyewall sonde will more often than not fail to sample these updrafts, it is apparently not very difficult to detect such an event, given a reasonable number of sondes.

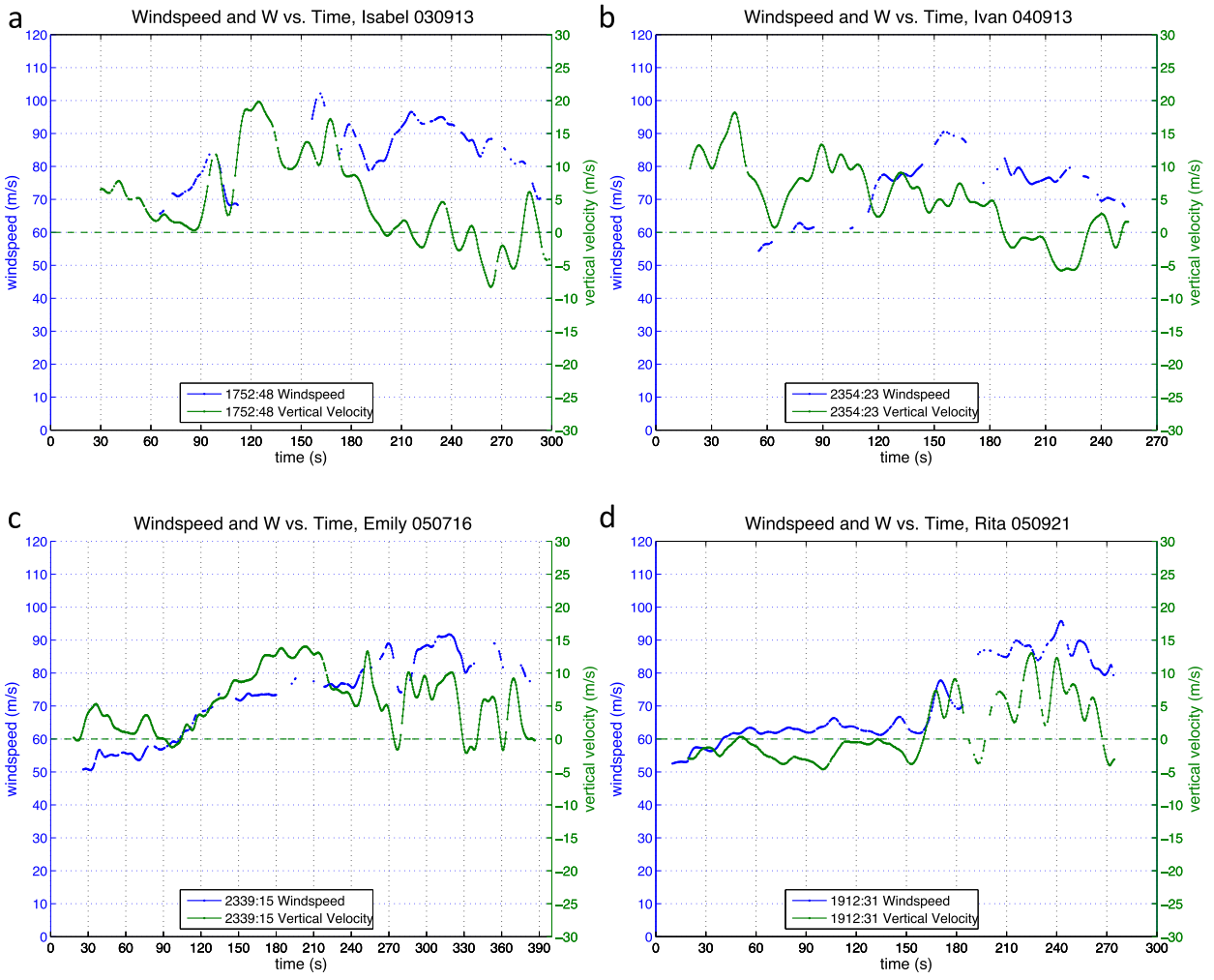

FIG. 15. For the same sondes as in Figs. 13 and 14, time series of wind speed and vertical velocity. The green horizontal dashed line indicates $w = 0\,\mathrm{m\,s^{-1}}$.

Figure 16 shows the horizontal trajectories of eight sondes dropped within a 2-min period in the eyewall of Hurricane Isabel, overlaid on the radar reflectivity field at a time 9 s prior to the first drop. Because the sonde trajectories each span a period of 3–5 min, we are unable to associate the sondes with specific small-scale features of the reflectivity field. However, the overall structure of the eyewall does not change significantly over the 5–7-min period that these eight sondes are in the air (not shown), and so we can see that the first few sondes in the sequence were dropped right at the inner edge of the eyewall, as represented by the region of very sharp radial gradient of reflectivity. The sequence spans much of the width of the eyewall, with the final sonde dropped just outward of the region of highest reflectivity. During the leg on which these sondes were dropped, the plane was flying radially outward from the storm center. The first three sondes sampled updrafts exceeding $10\,\mathrm{m\,s^{-1}}$, as did the sixth sonde. Additionally, the second, third, and fourth sondes sampled wind speeds exceeding $90\,\mathrm{m\,s^{-1}}$. This can be seen in Fig. 17, which shows vertical profiles of vertical velocity and horizontal wind speed for all eight sondes. The first three w10 sondes exhibit updraft maxima at similar heights, from 1200 to 1400 m. It is possible that they might have sampled the same feature (as the third sonde was dropped only about 2 km outward of the first sonde), though this is uncertain. Also of note is that each of the wind speed profiles exhibits significant fluctuations on the order of $10\,\mathrm{m\,s^{-1}}$. Perhaps as a result of these fluctuations, the height of maximum wind speed varies greatly among the sondes, from about 100 to 1000 m.

Using the FLIGHT+ dataset of Vigh et al. (2016), we can examine the flight-level radial profiles in relation to

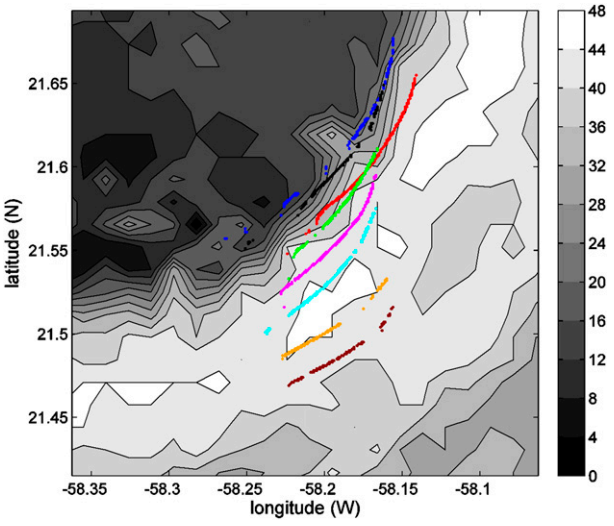

FIG. 16. Reflectivity (dBZ) from the lower fuselage radar at 1903:37 UTC 12 Sep 2003 in Hurricane Isabel, overlaid with the horizontal trajectories of eight dropsondes that were released within a 2-min period. This plot is zoomed in on the southeast quadrant of the eyewall, and the storm center is located at the upper-left corner. The radar reflectivity is from a time just prior (9 s) to the release of the first dropsonde. For this dropsonde sequence, the aircraft was flying outward from the center, and so the innermost sonde was released first. The drop times for the sondes can be seen in the legend of Fig. 17.

where the sondes were dropped. Figure 18 shows radial profiles of horizontal wind speed, vertical velocity, storm-relative radial velocity, temperature, and dewpoint (all data shown are at 1 Hz). Looking first at wind speed, it can be seen that the first five sondes were dropped inward of the peak flight-level wind speed, while the last three were dropped outward of the peak. From the temperature and dewpoint profiles, it is evident that the first four sondes were dropped within the clear air of the eye, whereas the fifth sonde was released at the inner edge of the eyewall cloud. The peak flight-level winds are therefore just barely within cloud. Wind speed is most variable between the second drop and the flight-level RMW, as is vertical velocity, which indicates that the flow is much more turbulent in the inner region of the eyewall than elsewhere. Across this 5-km region, the flight-level wind speed decreases inward by about 30 m s^{-1}. This radial shear is quite large, but even larger still is the vertical shear. The second sonde samples 90 m s^{-1} wind speed at about 1100 m, and so the winds increase with decreasing height by about 40 m s^{-1} over just 1 km. Either or both of these extreme shears might possibly contribute to the existence of small-scale vortices along the eye–eyewall interface.

A 30-s (about 4 km wide) region of continuous strong updraft is seen in the flight-level profile, nearly coincident with a region of very strong storm-relative outflow. The three w10 sondes at the beginning of the sequence were dropped in relatively weak vertical motion, with the first sonde actually in a downdraft. The strong sonde updrafts are about 1 km below and 1–3 km inward of the strong flight-level updraft, indicative of a substantial outward slope of the eyewall. The fourth and fifth sondes were released in strong updrafts (8–9 m s^{-1}), which can also be seen in the upper part of the dropsonde profiles. Though these sondes do not exceed the 10 m s^{-1} threshold, it is clear that they are part of the region of strong upward motion, and that the width of this region is comparable at and below flight level. If we were to use the Jorgensen et al. (1985) criteria for an updraft core (a continuous segment with w greater than 1 m s^{-1}), the flight-level updraft would be considered to be about 6 km wide. Note, however, that within this broader updraft, there are relatively large fluctuations (5–8 m s^{-1}) on the scale of 6–7 s (from peak to peak), or slightly less than a kilometer. These fluctuations may represent the perturbations associated with individual vortices, which are embedded within the broader updraft.

7. Discussion

It is often stated or implied that strong updrafts in tropical cyclones are relatively rare (Jorgensen et al. 1985; Black et al. 1994; Cecil and Zipser 1999; Jiang and Zipser 2006; Houze 2010; Rosenfeld et al. 2012; DeMaria et al. 2012; Dolling and Barnes 2012). Sometimes, the basis for this claim is that when examining vertical motions over the whole tropical cyclone, the percentage area covered by strong updrafts is small (e.g., Jorgensen et al. 1985). This is true, although we would argue that this is not the most useful metric, as it is currently well understood that outside the eyewall, the area covered by strong convection is relatively small, and as the area enclosed by a circle at large radius is much greater than the area of the eyewall, these statistics will mask the structure of the eyewall and its propensity for strong updrafts.

While the area covered by extreme updrafts in the eyewall is still likely to be relatively small, there is substantial evidence that for intense tropical cyclones, such updrafts are almost always present somewhere. The ubiquity of these features is evident from the fact that there have been nine Atlantic category 5 TCs during 1997–2013, and all nine had at least one extreme updraft sampled by a dropsonde, while at category 5 intensity. Of the 27 Atlantic TCs that peaked at category 4 in this same period, 16 had at least one extreme updraft within 12 h of a best track time with category 4 intensity. Of the 11 other storms, 4 were never observed by aircraft and 1

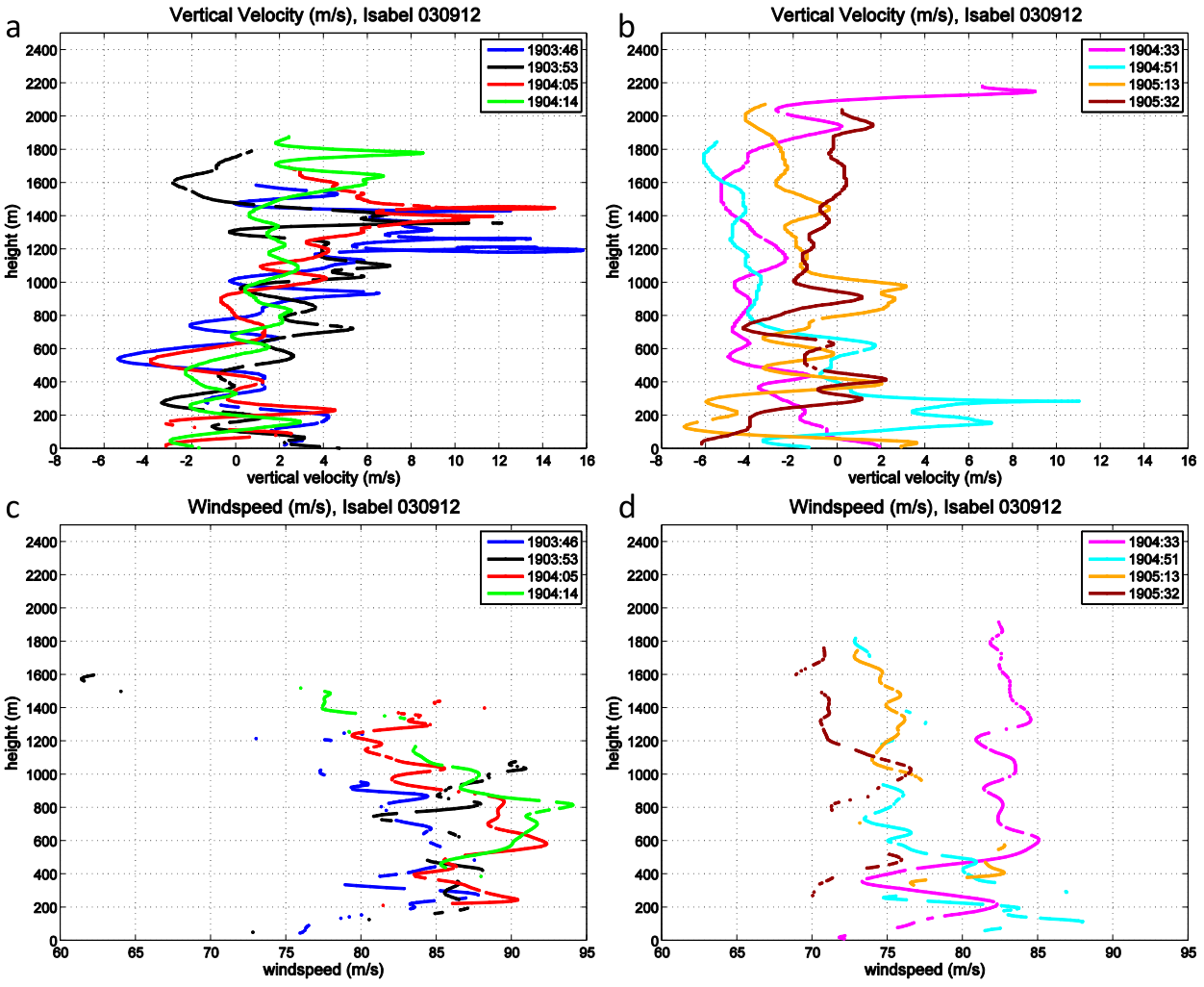

FIG. 17. Vertical profiles of (a),(b) vertical velocity and (c),(d) wind speed, for the eight Isabel sondes shown in Fig. 16. The drop times are given in the legends, and the colors correspond to those in Fig. 16.

was not observed during the period of peak intensity. Most of the remaining storms were only observed by USAF, which typically dropped only 4–8 sondes during a mission. Because of sampling biases, it is difficult to quantitatively estimate the area covered by extreme updrafts, or their true frequency as a function of intensity. Some storms were much more intensively sampled, and these storms tend to be very strong. On the other hand, among all TCs there are a greater number of weak storms, and this sampling effect appears to be dominant; from Wang et al. (2015), about twice as many sondes have been dropped by P3s in category 1–3 storms as compared to categories 4–5. Therefore, we believe that the result that extreme updrafts are found much more often in intense TCs is robust. It is also clear that for intense tropical cyclones, the presence of extreme updrafts at low levels is not at all unusual.

It has been known for some time that vertical wind shear systematically organizes vertical motion in tropical cyclones (e.g., Frank and Ritchie 1999; Black et al. 2002; Corbosiero and Molinari 2002; CM03; Reasor et al. 2009, 2013). While there is some variability in results among these (and other) studies, they generally have found that within the inner core region, updrafts preferentially occur downshear or in the downshear-left quadrant. Our results differ somewhat, in that while the extreme updrafts do occur preferentially in the downshear-left quadrant, they also occur preferentially (and with slightly greater frequency) in the upshear-left quadrant. None of these other studies found a preference for the upshear-left quadrant, and several of them found a secondary preference for the downshear-right quadrant, which contains few extreme updrafts in our dataset. It is possible that limited and/or biased sampling

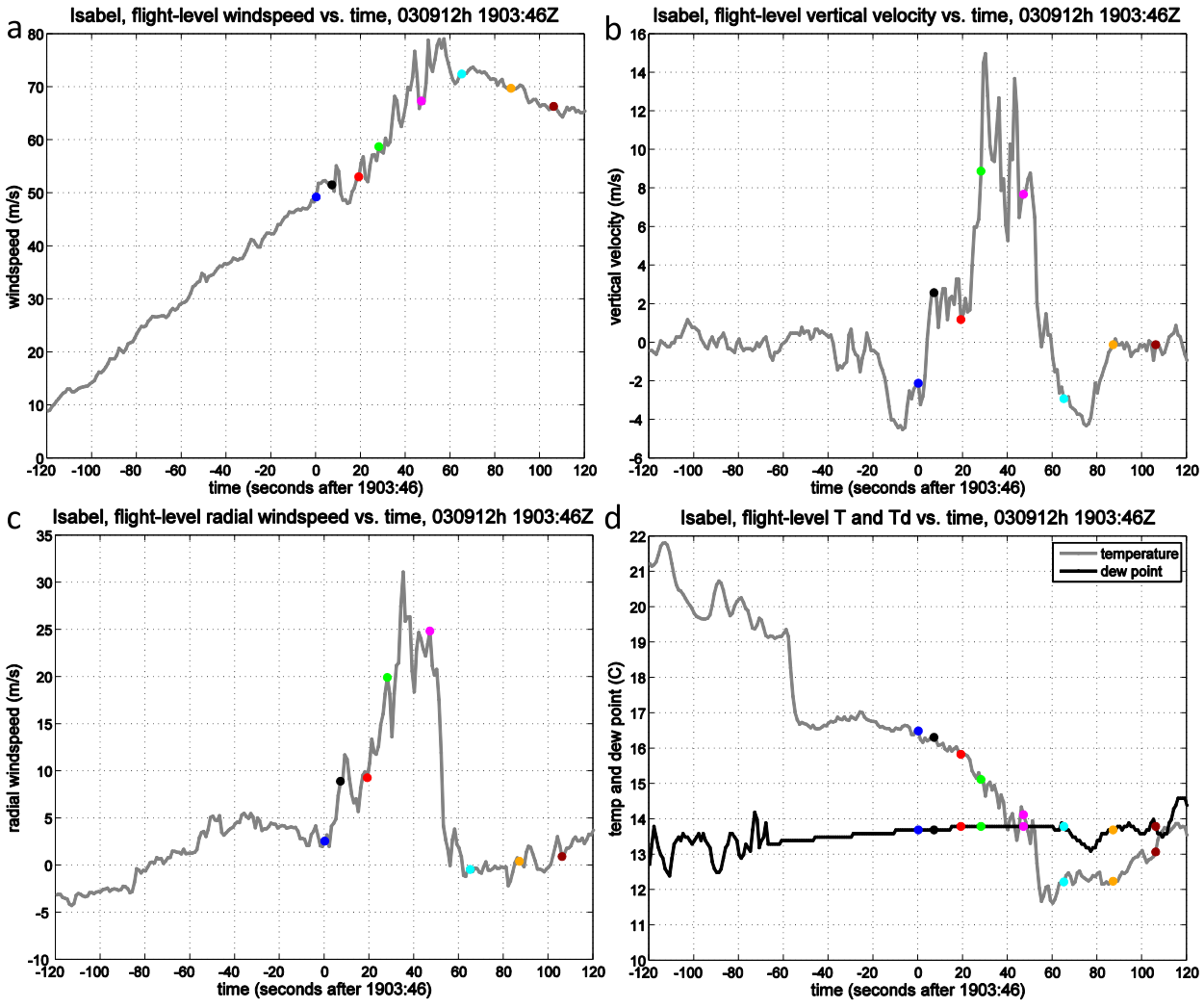

FIG. 18. Radial profiles of flight-level (a) wind speed, (b) vertical velocity, (c) storm-relative radial velocity, and (d) temperature and dewpoint, for the leg corresponding to the release of the sondes shown in Figs. 16 and 17. On each profile, the time at which each dropsonde was released is indicated with a dot, with the respective color corresponding to those in Figs. 16 and 17. Each plot spans 4 min in time (about 30-km distance), and is centered on the time that the first sonde in the sequence was released (1903:46 UTC). For (d), there is a region where dewpoint exceeds temperature, and this is indicative of spurious supersaturation as a result of sensor wetting (Eastin et al. 2002a,b). For the time period of this figure, the flight-level altitude varied from approximately 2100 to 2400 m.

could contribute somewhat to this discrepancy. It is also possible that the differences reflect the fact that we are examining a different population of updrafts than in these prior studies. Most previous studies that undertook a systematic examination of the shear-relative distribution of convection were focused primarily on midlevels (e.g., CM03; Reasor et al. 2013). It may be the case that low-level updrafts have a slightly different distribution than those at midlevels. Note that the peak frequency of low-level extreme updrafts in our dataset is downstream of the peak frequency in the aforementioned studies. This makes it unlikely that the location of the midlevel maximum in those studies is a simple consequence of the low-level features being advected by the mean tangential flow, as this advection would be in the wrong direction.

We have demonstrated that the extreme low-level updrafts cannot plausibly be explained by thermal buoyancy. If buoyancy is not responsible for the existence of the extreme low-level updrafts, then what is? The remaining alternative is the nonhydrostatic vertical pressure gradient force, which is associated primarily with gradients in the velocity field. It is not possible to assess this process from the dropsondes, but we can infer that such forcing is likely related to the existence of large localized vorticity (e.g., Markowski and Richardson

2010), which clearly is present in these events, considering the extreme gradients in horizontal wind speed that are evident in a number of dropsonde profiles. We hypothesize that the extreme low-level updrafts and wind speeds in our dataset are related to each other, and are in turn both related to kilometer-scale vortices that lie along the eye–eyewall interface. Marks et al. (2008) examined such a vortex that the NOAA P3 aircraft directly penetrated in Hurricane Hugo (1989). They determined that the diameter of the vortex at flight level (450-m height) was approximately 1 km, and had an associated tangential wind perturbation of 23 m s^{-1}. The peak positive wind speed perturbation associated with this vorticity maximum was found to be nearly coincident with a 21 m s^{-1} updraft, and the aircraft flew through several strong updraft–downdraft couplets as it traversed the eyewall. We believe it is possible that many of the dropsondes within our dataset sampled similar features as that described in Marks et al. (2008). We showed (Fig. 5) that the extreme low-level updrafts are almost exclusively found in a narrow zone on the inner edge of the eyewall, inward of the flight-level RMW, and this is also consistent with the feature described in Marks et al. (2008). Those authors noted that although their study was the first to describe in situ observations of this type of kilometer-scale vortex in tropical cyclones, such phenomena are ''likely more common than previously believed'' (p. 1253). We agree with this statement, and suggest that such vortices (and associated localized extreme updrafts and wind speeds) may be ubiquitous within the low-level eyewall of intense (category 4–5) tropical cyclones.

8. Summary and future work

a. Summary

In this study, we examined all available (about 12 000) dropsondes released within tropical cyclones during 1997–2013 in order to find and analyze the most extreme updrafts and horizontal wind speeds. After extensive automatic and manual quality control, we created a dataset of 169 sondes that sampled updrafts exceeding 10 m s^{-1} and 64 sondes that sampled wind speeds exceeding 90 m s^{-1}. Our primary findings are as follows:

(i) Extreme low-level updrafts are much more commonly observed within intense (category 4 and 5) TCs than within weaker storms. There is no obvious relationship with intensity change.
(ii) For sufficiently strong storms, these extreme updrafts are likely ubiquitous within the inner core.
(iii) Extreme updrafts are found across a broad range of heights below the typical flight level of 2–3 km. In contrast, the range of heights for extreme wind speeds is more restricted, with all wind maxima below 1500 m, and a pronounced peak in the distribution from 400- to 600-m height.
(iv) For both datasets, there are a number of sondes where the respective peak is found only a few hundred meters above the surface.
(v) Both extreme updrafts and wind speeds are nearly exclusively found in the eyewall, and within 10 km inward of the flight-level RMW.
(vi) The azimuthal distribution of both extreme updrafts and wind speeds are strongly related to both the direction of storm motion and the direction of the environmental vertical wind shear vector. The relationship with shear orientation is dominant, with about 80% of the w10 and ws90 sondes found in the left-of-shear semicircle.
(vii) The extreme low-level updrafts are *not* driven by buoyancy, as the required temperature perturbations would be implausibly large.

b. Additional questions and future work

This study suggests a number of additional questions that we are unable to answer with dropsondes alone. Dropsonde profiles represent a time series of point measurements as the sondes fall while being advected by the three-dimensional flow. Therefore, it is not possible to determine the time evolution of these updrafts, or even to assess their instantaneous spatial structure. Further, it is not at all clear what exactly is being sampled when a dropsonde encounters one of these extreme updrafts or wind maxima. The profiles are not actually vertical, and in fact, the typical sonde dropped within the eyewall is advected much farther azimuthally than it falls vertically. When the radius of the eyewall is small, some sondes will move halfway around the eyewall in the time it takes them to reach the surface. Therefore, it is possible that the very large gradients of both kinematic and thermodynamic variables within some sonde profiles do not actually represent vertical variations, but instead are primarily horizontal variations. This fact has important implications for how dropsonde profiles are interpreted. As pointed out by a reviewer, many previous observational studies of vertical motion in tropical cyclones (e.g., Jorgensen et al. 1985; Black et al. 1994, 1996; Guimond et al. 2010; Heymsfield et al. 2010) assumed that they were focusing specifically on deep, coherent updrafts. As implied in the above discussion, it is simply not possible to reliably estimate the depth and width of the features that are sampled by the dropsondes. Therefore, we cannot determine how the low-level updrafts we examine in this study are related to the population of updrafts examined in earlier flight-level and radar studies.

It is clear that the direction of environmental vertical wind shear strongly modulates the distribution of both low-level extreme updrafts and wind speeds. In our view, it is unclear as to why. There are a variety of ideas for how environmental shear controls the azimuthal distribution of convection in TCs (e.g., Jones 1995; Bender 1997; Frank and Ritchie 1999), but common to all extant theories is that shear-induced vertical motion is a response to TC-scale disruptions of thermal wind balance. The ascent that is induced downshear left is essentially a quasigeostrophic response (Davis et al. 2008), and therefore such ascent is weak and widespread. In current theories, this modulation of mesoscale ascent/descent in turn affects the distribution of localized strong updrafts by either favoring or suppressing buoyant convection (e.g., Davis et al. 2008), in a manner analogous to how midlatitude thunderstorms can be triggered or suppressed by large-scale lift or subsidence, respectively (Raymond and Jiang 1990; Trier et al. 2000). This idea works so long as the updrafts are buoyantly driven. However, we have shown that these extreme low-level updrafts are not forced by buoyancy. Therefore, the mechanism by which environmental vertical shear apparently controls the distribution of these updrafts seems unclear, as it is not obvious how or why weak mesoscale ascent/descent favors/suppresses dynamically forced updrafts. Assuming that vortices along the eye–eyewall interface are ultimately a manifestation of a (local) shear instability (which is our hypothesis), perhaps the environmental vertical wind shear modulates the structure of the mesoscale gradients of tangential, radial, and/or vertical velocity in such a manner as to preferentially support/suppress this instability.

Our ultimate goal is to understand the structure and dynamics of the small-scale vortices that have been observed within the low-level eyewall of intense tropical cyclones (Marks et al. 2008), which we believe our datasets presented here have sampled. We would also like to determine whether and how these features affect the overall storm intensity and mean structure. Finally, it is apparent that extremely intense wind speeds of 90–110 $\mathrm{m\,s^{-1}}$ can exist very close to the surface within tropical cyclones, and the observations we presented here represent some of the strongest near-surface wind speeds seen anywhere on earth. Such winds obviously pose a tremendous hazard to life and property in the case of landfall. Catastrophic damage from landfalling tropical cyclones can be extremely localized (e.g., Wakimoto and Black 1994; Powell and Houston 1996), and we speculate that the small-scale vortices along the eye–eyewall interface might be related to this phenomenon. It is therefore important to determine the frequency of such extreme near-surface wind maxima, and to quantify any dependence on storm intensity and structure.

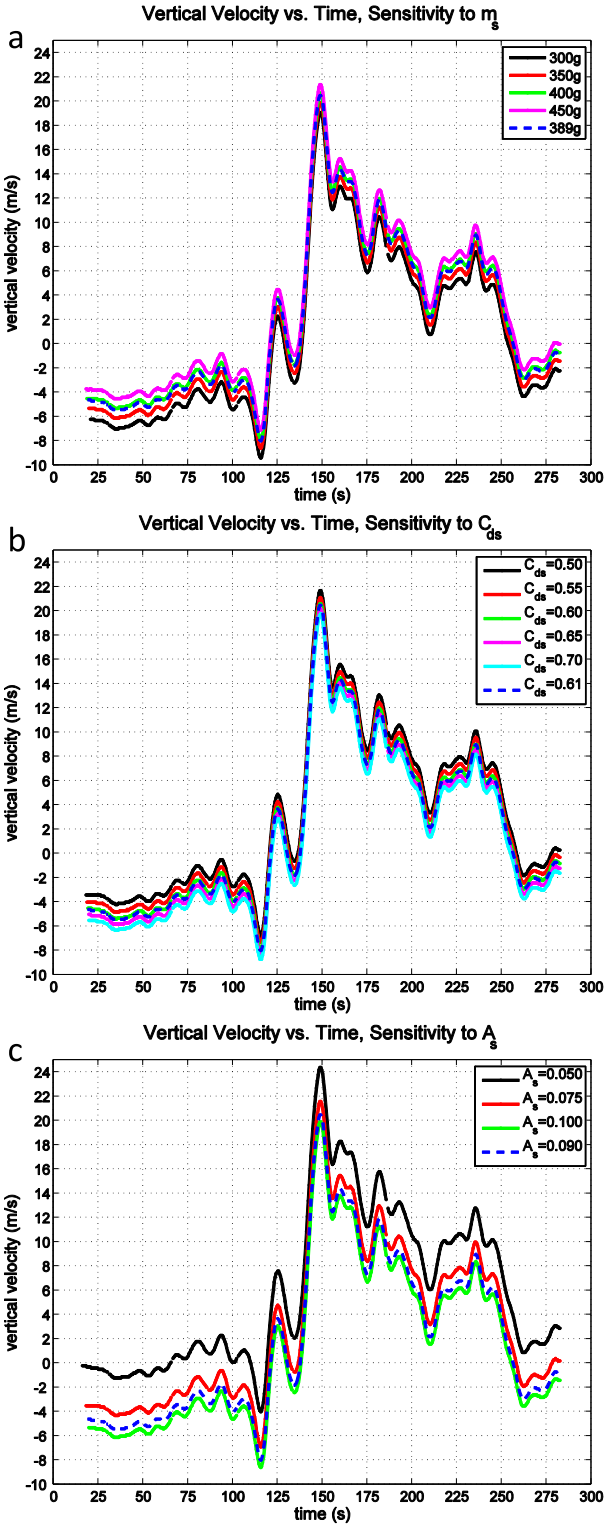

FIG. A1. Vertical velocity vs time for the Ivan sonde shown in Fig. 11c. Time series are shown for varying (a) m_s, (b) C_{ds}, and (c) A_s. For each panel, the respective parameter value used in previous figures for all RD93 sondes is indicated by the dashed blue line.

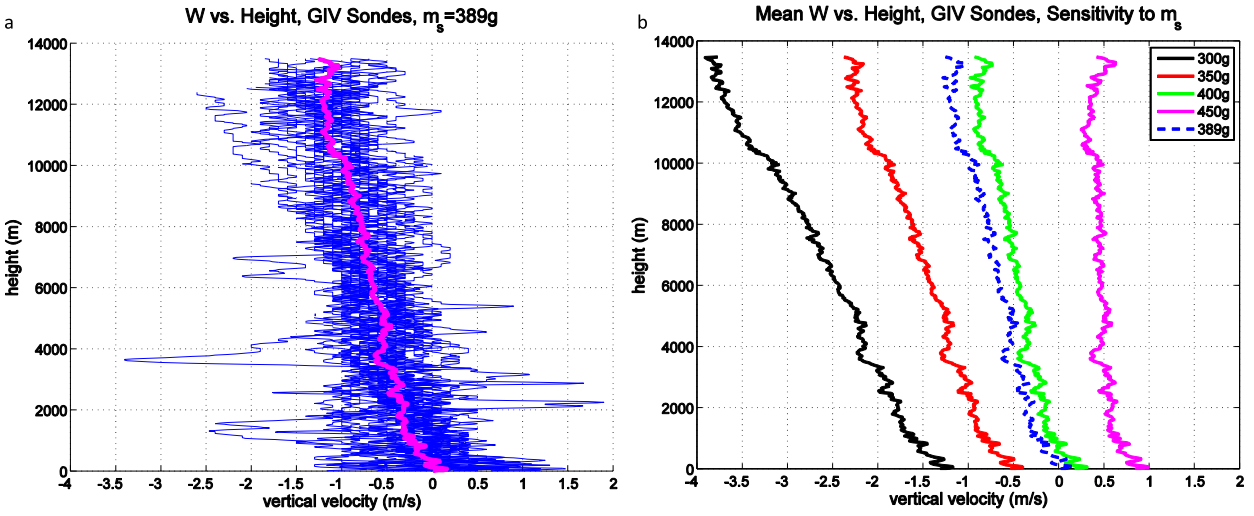

FIG. A2. (a) Vertical velocity vs height for 25 GIV sondes dropped in the environment of Ivan, at approximately the same time as the USAF sonde shown in Fig. A1. Blue lines represent individual sonde profiles, and the thick magenta line is the mean. Here, m_s is set to 389 g. (b) Mean vertical velocity vs height for the same 25 sondes, varying m_s. The dashed blue line in (b) is identical to the solid magenta line in (a), and represents the same sonde parameter settings as used for all RD93 sondes in this study.

Because observational sampling is inherently limited, it is not possible to address all of these issues from the dropsondes alone. Therefore, we plan to investigate these issues using large-eddy simulations, which are able to resolve the kilometer-scale vortices that the dropsondes may have sampled. Through these simulations, we should gain further insight into the structure and dynamics of these features, and to answer the questions we have raised above.

Acknowledgments. This research was performed at NCAR while the first author was an NSF-AGS Postdoctoral Fellow (Award 1231193). We thank Charlie Martin of NCAR's Earth Observing Laboratory (EOL) for invaluable assistance with the ASPEN software, and Kate Young and June Wang of NCAR/EOL for providing helpful dropsonde information. We also thank Jonathan Vigh for providing us access to his FLIGHT+ dataset, Chris Davis for helpful comments and suggestions on an earlier version of this manuscript, and Matt Eastin for helpful discussions regarding dropsonde quality control. We thank Matt Eastin and two anonymous reviewers for providing thorough reviews that greatly improved the manuscript.

APPENDIX

Sensitivity of Vertical Velocity to Sonde Characteristics

As discussed in section 2, there are several parameters with varying degrees of uncertainty that affect the calculated vertical velocity w, through the semiempirical formula for the terminal fall speed of the sonde, w_{fall}. From (1), these parameters are the sonde mass m_s, drag coefficient C_{ds}, and parachute area A_s. Here, we quantitatively evaluate the sensitivity of w to these three parameters. We first show this for a single example, using the same sonde from Hurricane Ivan (2004) as shown in Fig. 11c. Figure A1 shows vertical velocity versus time, for m_s varying from 300 to 450 g, for C_{ds} varying from 0.50 to 0.70, and for A_s varying from 0.05 to 0.10 m^2. Across these parameter ranges, the peak w varies by 2.3, 1.9, and 4.5 m s^{-1}, respectively. Note that this is merely illustrative of the sensitivity, and not necessarily representative of the actual uncertainty. The actual uncertainty depends on the degree of uncertainty in the parameters themselves; this is not completely known, but we have chosen a parameter space that we believe is substantially broader than the actual uncertainty.

From (1), w_{fall} has the same sensitivity for equivalent fractional changes in all three parameters. Note that the absolute sensitivity is independent of w itself, and so therefore the fractional uncertainty in w decreases with increasing w. This is why the dropsondes can be reliably used to measure extreme updrafts, but not the weak vertical motion that characterizes the eye or the environment far from the storm center.

As a further investigation of the uncertainty in w associated with sonde parameter uncertainty, Fig. A2 shows vertical velocity versus height, using the default parameter values given in section 2, for 25 sondes dropped by the NOAA GIV aircraft in the environment of Hurricane Ivan at approximately the same time as the USAF sonde shown in Fig. A1. For these sondes,

ASPEN was run in batch mode and no manual quality control was performed; four sondes that ASPEN indicated may contain errors were excluded. The GIV operates in the environment around the storm, away from convection, and so the true vertical velocity from GIV sondes is on average expected to be near zero. The calculated w for these sondes is indeed small, although values of around $-1\,\mathrm{m\,s^{-1}}$ are evident in the upper troposphere. Figure A2b shows the mean vertical velocity profile for these 25 sondes, varying m_s. For the default m_s of 389 g, the mean w appears to be biased low in the upper troposphere, while it is close to zero (and presumably relatively unbiased) at low levels. Lower values of m_s yield larger negative biases at upper levels, while $m_s = 450$ g yields a small positive bias at all levels. It is clear that for the default values of the parameters in (1), the bias in vertical velocity at low levels associated with sonde parameter uncertainty is less than $1\,\mathrm{m\,s^{-1}}$.

REFERENCES

Aberson, S. D., and D. P. Stern, 2006: Extreme horizontal winds measured by dropwindsondes in hurricanes. *27th Conf. on Hurricanes and Tropical Meteorology*, Monterey, CA, Amer. Meteor. Soc., 16.7. [Available online at https://ams.confex.com/ams/pdfpapers/108595.pdf.]

——, M. T. Montgomery, M. Bell, and M. Black, 2006: Hurricane Isabel (2003): New insights into the physics of intense storms. Part II: Extreme localized wind. *Bull. Amer. Meteor. Soc.*, **87**, 1349–1354, doi:10.1175/BAMS-87-10-1349.

Bender, M. A., 1997: The effect of relative flow on the asymmetric structure in the interior of hurricanes. *J. Atmos. Sci.*, **54**, 703–724, doi:10.1175/1520-0469(1997)054<0703:TEORFO>2.0.CO;2.

Black, M. L., R. W. Burpee, and F. D. Marks Jr., 1996: Vertical motion characteristics of tropical cyclones determined with airborne Doppler radial velocities. *J. Atmos. Sci.*, **53**, 1887–1909, doi:10.1175/1520-0469(1996)053<1887:VMCOTC>2.0.CO;2.

——, J. F. Gamache, F. D. Marks Jr., C. E. Samsury, and H. E. Willoughby, 2002: Eastern Pacific Hurricanes Jimena of 1991 and Olivia of 1994: The effect of vertical shear on structure and intensity. *Mon. Wea. Rev.*, **130**, 2291–2312, doi:10.1175/1520-0493(2002)130<2291:EPHJOA>2.0.CO;2.

Black, R. A., H. B. Bluestein, and M. L. Black, 1994: Unusually strong vertical motions in a Caribbean hurricane. *Mon. Wea. Rev.*, **122**, 2722–2739, doi:10.1175/1520-0493(1994)122<2722:USVMIA>2.0.CO;2.

Braun, S. A., 2002: A cloud-resolving simulation of Hurricane Bob (1991): Storm structure and eyewall buoyancy. *Mon. Wea. Rev.*, **130**, 1573–1592, doi:10.1175/1520-0493(2002)130<1573:ACRSOH>2.0.CO;2.

Cecil, D. J., and E. J. Zipser, 1999: Relationships between tropical cyclone intensity and satellite-based indicators of inner core convection: 85-GHz ice-scattering signature and lightning. *Mon. Wea. Rev.*, **127**, 103–123, doi:10.1175/1520-0493(1999)127<0103:RBTCIA>2.0.CO;2.

Corbosiero, K. L., and J. Molinari, 2002: The effects of vertical wind shear on the distribution of convection in tropical cyclones. *Mon. Wea. Rev.*, **130**, 2110–2123, doi:10.1175/1520-0493(2002)130<2110:TEOVWS>2.0.CO;2.

——, and ——, 2003: The relationship between storm motion, vertical wind shear, and convective asymmetries in tropical cyclones. *J. Atmos. Sci.*, **60**, 366–376, doi:10.1175/1520-0469(2003)060<0366:TRBSMV>2.0.CO;2.

Davis, C., S. C. Jones, and M. Riemer, 2008: Hurricane vortex dynamics during Atlantic extratropical transition. *J. Atmos. Sci.*, **65**, 714–736, doi:10.1175/2007JAS2488.1.

DeMaria, M., M. Mainelli, L. K. Shay, J. A. Knaff, and J. Kaplan, 2005: Further improvements to the Statistical Hurricane Intensity Prediction Scheme (SHIPS). *Wea. Forecasting*, **20**, 531–543, doi:10.1175/WAF862.1.

——, R. T. DeMaria, J. A. Knaff, and D. Molenar, 2012: Tropical cyclone lightning and rapid intensity change. *Mon. Wea. Rev.*, **140**, 1828–1842, doi:10.1175/MWR-D-11-00236.1.

Dolling, K. P., and G. M. Barnes, 2012: The creation of a high equivalent potential temperature reservoir in Tropical Storm Humberto (2001) and its possible role in storm deepening. *Mon. Wea. Rev.*, **140**, 492–505, doi:10.1175/MWR-D-11-00068.1.

Doswell, C. A., III, and P. M. Markowski, 2004: Is buoyancy a relative quantity? *Mon. Wea. Rev.*, **132**, 853–863, doi:10.1175/1520-0493(2004)132<0853:IBARQ>2.0.CO;2.

Eastin, M. D., P. G. Black, and W. M. Gray, 2002a: Flight-level thermodynamic instrument wetting errors in hurricanes. Part I: Observations. *Mon. Wea. Rev.*, **130**, 825–841, doi:10.1175/1520-0493(2002)130<0825:FLTIWE>2.0.CO;2.

——, ——, and ——, 2002b: Flight-level thermodynamic instrument wetting errors in hurricanes. Part II: Implications. *Mon. Wea. Rev.*, **130**, 842–851, doi:10.1175/1520-0493(2002)130<0842:FLTIWE>2.0.CO;2.

——, W. M. Gray, and P. G. Black, 2005a: Buoyancy of convective vertical motions in the inner core of intense hurricanes. Part I: General statistics. *Mon. Wea. Rev.*, **133**, 188–208, doi:10.1175/MWR-2848.1.

——, ——, and ——, 2005b: Buoyancy of convective vertical motions in the inner core of intense hurricanes. Part II: Case studies. *Mon. Wea. Rev.*, **133**, 209–227, doi:10.1175/MWR-2849.1.

Frank, W. M., and E. A. Ritchie, 1999: Effects of environmental flow upon tropical cyclone structure. *Mon. Wea. Rev.*, **127**, 2044–2061, doi:10.1175/1520-0493(1999)127<2044:EOEFUT>2.0.CO;2.

Franklin, J. L., M. L. Black, and K. Valde, 2003: GPS dropwindsonde wind profiles in hurricanes and their operational implications. *Wea. Forecasting*, **18**, 32–44, doi:10.1175/1520-0434(2003)018<0032:GDWPIH>2.0.CO;2.

Guimond, S. R., G. M. Heymsfield, and F. J. Turk, 2010: Multiscale observations of Hurricane Dennis (2005): The effects of hot towers on rapid intensification. *J. Atmos. Sci.*, **67**, 633–654, doi:10.1175/2009JAS3119.1.

Heymsfield, G. M., L. Tian, A. J. Heymsfield, L. Li, and S. Guimond, 2010: Characteristics of deep tropical and subtropical convection from nadir-viewing high-altitude airborne Doppler radar. *J. Atmos. Sci.*, **67**, 285–308, doi:10.1175/2009JAS3132.1.

Hock, T. F., and J. L. Franklin, 1999: The NCAR GPS dropwindsonde. *Bull. Amer. Meteor. Soc.*, **80**, 407–420, doi:10.1175/1520-0477(1999)080<0407:TNGD>2.0.CO;2.

Houze, R. A., Jr., 2010: Clouds in tropical cyclones. *Mon. Wea. Rev.*, **138**, 293–344, doi:10.1175/2009MWR2989.1.

Jiang, H., and E. J. Zipser, 2006: Retrieval of hydrometeor profiles in tropical cyclones and convection from combined radar and radiometer observations. *J. Appl. Meteor. Climatol.*, **45**, 1096–1115, doi:10.1175/JAM2386.1.

Jones, S. C., 1995: The evolution of vortices in vertical shear. I: Initially barotropic vortices. *Quart. J. Roy. Meteor. Soc.*, **121**, 821–851, doi:10.1002/qj.49712152406.

Jorgensen, D. P., and M. A. LeMone, 1989: Vertical velocity characteristics of oceanic convection. *J. Atmos. Sci.*, **46**, 621–640, doi:10.1175/1520-0469(1989)046<0621:VVCOOC>2.0.CO;2.

——, E. J. Zipser, and M. A. LeMone, 1985: Vertical motions in intense hurricanes. *J. Atmos. Sci.*, **42**, 839–856, doi:10.1175/1520-0469(1985)042<0839:VMIIH>2.0.CO;2.

Kaplan, J., and M. DeMaria, 2003: Large-scale characteristics of rapidly intensifying tropical cyclones in the North Atlantic basin. *Wea. Forecasting*, **18**, 1093–1108, doi:10.1175/1520-0434(2003)018<1093:LCORIT>2.0.CO;2.

Kimball, S. K., and M. S. Mulekar, 2004: A 15-year climatology of North Atlantic tropical cyclones. Part I: Size parameters. *J. Climate*, **17**, 3555–3575, doi:10.1175/1520-0442(2004)017<3555:AYCONA>2.0.CO;2.

Landsea, C. W., and J. L. Franklin, 2013: Atlantic hurricane database uncertainty and presentation of a new database format. *Mon. Wea. Rev.*, **141**, 3576–3592, doi:10.1175/MWR-D-12-00254.1.

LeMone, M. A., and E. J. Zipser, 1980: Cumulonimbus vertical velocity events in GATE. Part I: Diameter, intensity, and mass flux. *J. Atmos. Sci.*, **37**, 2444–2457, doi:10.1175/1520-0469(1980)037<2444:CVVEIG>2.0.CO;2.

Lorsolo, S., J. A. Zhang, F. Marks Jr., and J. Gamache, 2010: Estimation and mapping of hurricane turbulent energy using airborne Doppler measurements. *Mon. Wea. Rev.*, **138**, 3656–3670, doi:10.1175/2010MWR3183.1.

Markowski, P., and Y. Richardson, 2010: *Mesoscale Meteorology in Midlatitudes*. Wiley-Blackwell, 430 pp.

Marks, F. D., P. G. Black, M. T. Montgomery, and R. W. Burpee, 2008: Structure of the eye and eyewall of Hurricane Hugo (1989). *Mon. Wea. Rev.*, **136**, 1237–1259, doi:10.1175/2007MWR2073.1.

Persing, J., M. T. Montgomery, J. C. McWilliams, and R. K. Smith, 2013: Asymmetric and axisymmetric dynamics of tropical cyclones. *Atmos. Chem. Phys.*, **13**, 12 299–12 341, doi:10.5194/acp-13-12299-2013.

Powell, M. D., and S. H. Houston, 1996: Hurricane Andrew's landfall in South Florida. Part II: Surface wind fields and potential real-time applications. *Wea. Forecasting*, **11**, 329–349, doi:10.1175/1520-0434(1996)011<0329:HALISF>2.0.CO;2.

Raymond, D. J., and H. Jiang, 1990: A theory for long-lived mesoscale convective systems. *J. Atmos. Sci.*, **47**, 3067–3077, doi:10.1175/1520-0469(1990)047<3067:ATFLLM>2.0.CO;2.

Reasor, P. D., M. D. Eastin, and J. F. Gamach, 2009: Rapidly intensifying Hurricane Guillermo (1997). Part I: Low-wavenumber structure and evolution. *Mon. Wea. Rev.*, **137**, 603–631, doi:10.1175/2008MWR2487.1.

——, R. Rogers, and S. Lorsolo, 2013: Environmental flow impacts on tropical cyclone structure diagnosed from airborne Doppler radar composites. *Mon. Wea. Rev.*, **141**, 2949–2969, doi:10.1175/MWR-D-12-00334.1.

Rose, S., P. Jaramillo, M. J. Small, I. Grossmann, and J. Apt, 2012: Quantifying the hurricane risk to offshore wind turbines. *Proc. Natl. Acad. Sci. USA*, **109**, 3247–3252, doi:10.1073/pnas.1111769109.

Rosenfeld, D., W. L. Woodley, A. Khain, W. R. Cotton, G. Carrió, I. Ginis, and J. H. Golden, 2012: Aerosol effects on microstructure and intensity of tropical cyclones. *Bull. Amer. Meteor. Soc.*, **93**, 987–1001, doi:10.1175/BAMS-D-11-00147.1.

Rotunno, R., Y. Chen, W. Wang, C. Davis, J. Dudhia, and G. J. Holland, 2009: Large-eddy simulation of an idealized tropical cyclone. *Bull. Amer. Meteor. Soc.*, **90**, 1783–1788, doi:10.1175/2009BAMS2884.1.

Smith, R. K., M. T. Montgomery, and H. Zhu, 2005: Buoyancy in tropical cyclones and other rapidly rotating atmospheric vortices. *Dyn. Atmos. Oceans*, **40**, 189–208, doi:10.1016/j.dynatmoce.2005.03.003.

Stern, D. P., and S. D. Aberson, 2006: Extreme vertical winds measured by dropwindsondes in hurricanes. *27th Conf. on Hurricanes and Tropical Meteorology*, Monterey, CA, Amer. Meteor. Soc., 16B.8. [Available online at https://ams.confex.com/ams/27Hurricanes/techprogram/paper_108766.htm.]

——, J. L. Vigh, D. S. Nolan, and F. Zhang, 2015: Revisiting the relationship between eyewall contraction and intensification. *J. Atmos. Sci.*, **72**, 1283–1306, doi:10.1175/JAS-D-14-0261.1.

Trier, S. B., C. A. Davis, and W. C. Skamarock, 2000: Long-lived mesoconvective vortices and their environment. Part II: Induced thermodynamic destabilization in idealized simulations. *Mon. Wea. Rev.*, **128**, 3396–3412, doi:10.1175/1520-0493(2000)128<3396:LLMVAT>2.0.CO;2.

Uhlhorn, E. W., and D. S. Nolan, 2012: Observational undersampling in tropical cyclones and implications for estimated intensity. *Mon. Wea. Rev.*, **140**, 825–840, doi:10.1175/MWR-D-11-00073.1.

Vigh, J. L., and Coauthors, 2016: FLIGHT+: The extended flight level dataset for tropical cyclones (version 1.0). Tropical Cyclone Data Project, National Center for Atmospheric Research, Research Applications Laboratory, Boulder, CO, accessed 21 January 2015, doi:10.5065/D6WS8R93.

Wakimoto, R. M., and P. G. Black, 1994: Damage survey of Hurricane Andrew and its relationship to the eyewall. *Bull. Amer. Meteor. Soc.*, **75**, 189–200, doi:10.1175/1520-0477(1994)075<0189:DSOHAA>2.0.CO;2.

Wang, J., J. Bian, W. O. Brown, H. Cole, V. Grubišić, and K. Young, 2009: Vertical air motion from T-REX radiosonde and dropsonde data. *J. Atmos. Oceanic Technol.*, **26**, 928–942, doi:10.1175/2008JTECHA1240.1.

——, and Coauthors, 2015: A long-term, high-quality, high-vertical-resolution GPS dropsonde dataset for hurricane and other studies. *Bull. Amer. Meteor. Soc.*, **96**, 961–973, doi:10.1175/BAMS-D-13-00203.1.

Willoughby, H. E., and M. B. Chelmow, 1982: Objective determination of hurricane tracks from aircraft observations. *Mon. Wea. Rev.*, **110**, 1298–1305, doi:10.1175/1520-0493(1982)110<1298:ODOHTF>2.0.CO;2.

Zhang, D.-L., Y. Liu, and M. K. Yau, 2000: A multiscale numerical study of Hurricane Andrew (1992). Part III: Dynamically induced vertical motion. *Mon. Wea. Rev.*, **128**, 3772–3788, doi:10.1175/1520-0493(2001)129<3772:AMNSOH>2.0.CO;2.

Zhang, J. A., F. D. Marks, M. T. Montgomery, and S. Lorsolo, 2011: An estimation of turbulent characteristics in the low-level region of intense hurricanes Allen (1980) and Hugo (1989). *Mon. Wea. Rev.*, **139**, 1447–1462, doi:10.1175/2010MWR3435.1.

Zipser, E. J., and M. A. LeMone, 1980: Cumulonimbus vertical velocity events in GATE. Part II: Synthesis and model core structure. *J. Atmos. Sci.*, **37**, 2458–2469, doi:10.1175/1520-0469(1980)037<2458:CVVEIG>2.0.CO;2.

——, C. Liu, D. J. Cecil, S. W. Nesbitt, and D. P. Yorty, 2006: Where are the most intense thunderstorms on Earth? *Bull. Amer. Meteor. Soc.*, **87**, 1057–1071, doi:10.1175/BAMS-87-8-1057.